This is a preprint, the final version is subject to change, of the American Mineralogist (MSA)
Cite as Authors (Year) Title. American Mineralogist, in press.
(DOI will not work until issue is live.) DOI: http://dx.doi.org/10.2138/am-2017-6039

Revision 1:

Revisiting the Nontronite Mössbauer Spectra

Fabien Baron[1,*], Sabine Petit[1], Martin Pentrák[2], Alain Decarreau[1], and Joseph W. Stucki[2]

[1]Institut de Chimie des Milieux et Matériaux de Poitiers (IC2MP), UMR CNRS 7285 Université de Poitiers, Poitiers, France

[2]Department of Natural Resources and Environmental Sciences, University of Illinois at Urbana–Champaign, Urbana, Illinois, USA

*corresponding author: Fabien Baron - fabien.baron@univ-poitiers.fr

ABSTRACT

The distribution of ferric iron (Fe(III)) between the octahedral and tetrahedral sheets of smectites is still an active problem due to the difficulty of identifying and quantifying the tetrahedral ferric iron ($^{[4]}$Fe(III)). Mössbauer spectroscopy has often been used to address this problem, with the spectra being fitted by a sum of doublets, but the empirical attribution of each doublet has failed to yield a uniform interpretation of the spectra of natural reference Fe(III)-rich smectites, especially with regard to $^{[4]}$Fe(III), because little consensus exists as to the $^{[4]}$Fe(III) content of natural samples. In an effort to resolve this problem, the current study was undertaken using a series of synthetic nontronites $[Si_{4-x}\ ^{[4]}Fe(III)_x]\ ^{[6]}Fe(III)_2O_{10}(OH)_2Na_x$ with x ranging from 0.43 to 1.3. Mössbauer spectra were obtained at 298, 77, and 4 K. Statistically acceptable deconvolutions of the Mössbauer spectra at 298 and 77 K were used to develop a model of the distribution of tetrahedral substitutions, taking into account: (i) the $^{[4]}$Fe(III) content; (ii) the three possible tetrahedral cationic environments around $^{[6]}$Fe(III), i.e., [4Si]-(3$^{[6]}$Fe(III)), [3Si $^{[4]}$Fe(III)]-(3$^{[6]}$Fe(III)), and [2Si 2$^{[4]}$Fe(III)]-(3$^{[6]}$Fe(III)); and (iii) the local environment around a $^{[4]}$Fe(III), i.e., [3Si]-(2$^{[6]}$Fe(III)) respecting Lowenstein's Rule. This approach allowed the range of Mössbauer parameters for $^{[6]}$Fe(III) and $^{[4]}$Fe(III) to be determined and then applied to spectra of natural Fe(III)-rich smectites. Results revealed the necessity of taking into account the distribution of tetrahedral cations ($^{[4]}$R(III)) around

28 $^{[6]}$Fe(III) cations in order to deconvolute the Mössbauer spectra, and also highlighted the
29 influence of sample crystallinity on Mössbauer parameters.
30
31 **KEYWORDS**
32 Clay minerals, Iron, Mössbauer spectroscopy, Nontronite, Smectites, Tetrahedral iron
33
34 **INTRODUCTION**
35 Iron (Fe) is a major element in terms of abundance in the Earth's crust. Many minerals
36 contain Fe and some of them, such as Fe (oxyhydr)oxides and Fe-bearing swelling clay
37 minerals, play a significant role in many natural processes occurring at the Earth's surface and
38 in its subsurface (Murad 2013; Stucki 2013). Virtually all swelling clay minerals, known as
39 smectites, contain Fe, and are ubiquitous in the Earth's surface. Fe can exist in the structure of
40 the smectites in either the ferrous (Fe(II)) or the ferric (Fe(III)) state. The structure of the
41 smectite layers consists of one central octahedral sheet that shares oxygens with two
42 tetrahedral sheets, one on each side. The cations in the octahedral sheet are coordinated by
43 four oxygens and two hydroxyl groups, while the cations in the tetrahedral sheets are
44 coordinated by four oxygens. The octahedral sheet consists of three different crystallographic
45 sites, two *cis* sites and one *trans* site relative to the hydroxyl group positions. In the case of
46 dioctahedral smectites, the octahedral sites are mainly occupied by trivalent cations (R(III))
47 (R = aluminum (Al) or Fe(III)) and only two-thirds of these sites are filled, whereas the
48 tetrahedral sites are mainly occupied by silicon (Si) cations. Heterovalent substitutions can
49 occur in both the tetrahedral (where Al or Fe(III) can substitute for Si) and the octahedral
50 (where magnesium (Mg), nickel (Ni(II)), or Fe(II) can substitute for Al or Fe(III)) sheets,
51 which creates a net negative charge on the smectite layer. The charge imbalance is generally
52 compensated by the incorporation of alkaline cations in the interlayer space. Nontronite is the

general name for the dioctahedral Fe(III)-rich end-member of the smectite clay minerals group.

The negative charge induced by heterovalent substitutions partially controls the physical-chemical properties of Fe(III)-rich smectites. Fe(III) has been observed in both tetrahedral and octahedral sites in the nontronite structure. The $^{[6]}$Fe(III) content is relatively easy to quantify, whereas quantifying the $^{[4]}$Fe(III) content has proven to be a challenge (Gates et al. 2002). Petit et al. (2015) and Baron et al. (2016) recently proposed several formulas to estimate the $^{[6]}$Fe(III) and $^{[4]}$Fe(III) contents, based on infrared spectroscopy from a series of synthetic smectites.

Mössbauer spectroscopy is used in clay science mainly for mineralogical identification of various Fe-containing phases (oxides, sulfides, sulfates, carbonates, and phosphates) and to study magnetic impurities (in particular Fe (oxyhydr)oxides), the oxidation state of Fe, and the location of Fe atoms in clay mineral samples (Murad 2013; Stucki 2013). It was used also for mineralogical identification of Fe (oxyhydr)oxides on Mars (Klingelhöfer et al. 2004, 2006; Morris et al. 2004; Schröder et al. 2011). The capability of this type of spectroscopy to identify silicate minerals remains a matter of debate due to the lack of specific features uniquely attributable to specific silicate minerals (Dyar and Schaefer 2008; Murad 2008).

Octahedral Fe(III)

The capability of Mössbauer spectroscopy to study the distribution of Fe(III) cations between both the octahedral and the tetrahedral sheets also remains uncertain (Cardile 1989; Dyar 1993; Rancourt 1993; Decarreau et al. 2008), but some progress has been made toward identifying the components attributable to $^{[6]}$Fe(III). The spectra of smectite samples containing only $^{[6]}$Fe(III) cations consist of at least two doublets (Goodman 1978; Heller-Kallai and Rozenson 1981; Daynyak and Drits 1987; Luca 1991; Cashion et al. 2008, 2010; Dyar et al. 2008). The origin of these two doublets was first attributed to Fe(III) cations in *cis*

and *trans* octahedral sites (Goodman et al. 1976; Heller-Kallai and Rozenson 1981; Cardile and Johnston 1985), but this interpretation is doubtful because several studies concluded that smectites containing a high $^{[6]}$Fe(III) content, like nontronite, are *trans* vacant (*tv*), meaning that $^{[6]}$Fe(III) cations are located only in *cis* sites in the octahedral sheet (Petit et al. 1992; Drits et al. 2006; Wolters et al. 2009). On the other hand, Lear and Stucki (1989) found that the magnetic ordering of Fe(III) in nontronites and ferruginous smectite was frustrated antiferromagnetic, which means that as much as 13% of the $^{[6]}$Fe(III) could be in *trans* sites. Even that result, however, would not allow for the assignment of the two Mössbauer doublets to *cis* and *trans* because the relative areas of the two $^{[6]}$Fe(III) doublets are much larger than the suggested 13% value.

Some authors proposed an alternative interpretation based on the local tetrahedral environments around *cis* $^{[6]}$Fe(III) cations (Goodman 1978; Besson et al. 1983; Daynyak and Drits 1987; Cashion et al. 2008, 2010; Decarreau et al. 2008). One of the doublets was attributed to $^{[6]}$Fe(III) surrounded by [4Si] in the tetrahedral sheet, and the other was attributed to a [3Si-R^{3+}] tetrahedral configuration.

Tetrahedral Fe(III)

A general consensus is that the doublet feature in the Mössbauer spectrum deriving from $^{[4]}$Fe(III) is characterized by a lower isomer shift (δ) than those for $^{[6]}$Fe(III) cations (Annersten et al. 1971; Goodman et al. 1976; Goodman 1978; Coey 1980; Besson et al. 1983; Daynyak and Drits 1987; Luca 1991; Decarreau et al. 2008). Empirical deconvolution has often been used to interpret the Mössbauer spectra and to determine the crystal chemistry of a smectite sample. However, this approach can involve some contradictory results (Cardile 1989). For example, for the Garfield nontronite, the $^{[4]}$Fe(III) amount was diversely estimated to be 9 atomic percent (at.%) of total Fe(III) (Goodman et al. 1976; Johnston and Cardile

1985), 2 at.% (Luca 1991), < 1 at.% (Bonnin et al. 1985), and absent due to lack of evidence (Rozenson and Heller-Kallai 1977).

Natural nontronite samples, which sometimes have complex co-existing mineralogy (quartz, iron oxide…) and bulk chemistry (Mg, Al…), and often contain only a small amount of $^{[4]}$Fe(III), are not really adapted to determine the Mössbauer parameters of Fe(III) cations. Nontronite synthesis, on the other hand, appears to be a valuable way to supply smectites with controlled Fe(III) contents and site occupancies. Synthetic Fe(III)-nontronites also had the ability to simplify the crystal structure, and avoided other interferences to site occupancies due to Al or Mg for Fe(III) substitutions.

The objective of the present paper was, thus, to test the hypothesis that proper assignment of Mössbauer spectral components deriving from both $^{[6]}$Fe(III) and $^{[4]}$Fe(III) can be achieved by analyzing a series of synthetic nontronites over a wide range of $^{[4]}$Fe(III) contents and known crystal chemistries (Baron et al. 2016).

MATERIALS AND METHODS

Synthetic nontronites

Six synthetic nontronites of the series described by Baron et al. (2016) were used in this study. These pure nontronites were selected to span a wide range of $^{[4]}$Fe(III) content (x), ranging from x=0.5 (sample NT0) to x=1.3 (sample NT7) moles per half unit cell $[Si_{4-x}{}^{[4]}Fe(III)_x]\ {}^{[6]}Fe(III)_2O_{10}(OH)_2Na_x$ (Table 1). The $^{[4]}$Fe(III) content (x) was obtained by chemical analyses using a Scanning Electron Microscope (SEM) equipped with an Energy Dispersive Spectrometer (EDS) and confirmed by infrared spectroscopy using the wavenumber of the stretching Si-O vibrations (Baron et al. 2016).

Mössbauer spectroscopy

Mössbauer spectra were recorded using a Web Research, Inc. (Edina, Minnesota) spectrometer equipped with a Janis model SHI-850-5 (Janis, Inc., Woburn, Massachusetts) closed-cycle, low-temperature cryostat at the University of Illinois. The velocity drive transducer operated in a triangular waveform mode over energy ranges of ± 11 or 4 mm s^{-1}, with a 50 mCi ^{57}Co source dispersed as 10 wt.% in a thin Rh foil (Ritverc, Inc. St. Petersburg, Russia). Calibration of the velocity scale was performed by measuring the magnetic hyperfine field (Bhf) of a 7 μm thick α-Fe foil at the sample temperatures, nominally at 298, 77, and 4 K (Stucki et al. 2014).

From the empirical deconvolutions of the Mössbauer spectra, the different proportions of each doublet based on doublet areas (%), saturation corrections, and recoil-free fraction effects were considered (De Grave and Van Alboom 1991; Dyar et al. 2008). Samples were analyzed in powder form and were mixed with confectioners' sugar, as needed, to achieve a density of 5 mg Fe/cm^2 of sampled area in order to achieve thin absorber status.

The same recoil-free fractions of doublets linked to $^{[6]}$Fe(III) and $^{[4]}$Fe(III) was assumed. Dyar et al. (2008) calculated similar recoil-free fraction values (0.917 and 0.916 at 80 K, and 0.823 and 0.821 at 298 K) for two doublets linked to $^{[6]}$Fe(III) for a nontronite sample. Moreover, De Grave and Van Alboom (1991) calculated similar recoil-free fraction values for doublets linked to $^{[6]}$Fe(III) and $^{[4]}$Fe(III) in ferridiopside. According to Dyar et al. (2008), the error on the relative percentage of the different cationic environments was ± 1 - 3%.

Spectral deconvolution of the Mössbauer spectra was performed using a sum of doublets having a Lorentzian peak shape (Murad and Cashion 2004). Rancourt (2004) argued, however, that a Voigt-based deconvolution was theoretically better than a deconvolution using Lorentzian peak shape. Pseudo-Voigt peak shape which generally approximates the Voigt peak-shape (Dyar et al. 2008) was also tested, but no better results were obtained. The

two peaks that composed a doublet were constrained to have the same width and the same area. Each doublet was characterized by an isomer shift (δ), a quadrupole splitting (Δ), a relative area (%), and a line width, all of which were adjustable parameters. The fitting procedure was based on the refinement of all parameters of each doublet using the least-squares method. The quality of the fit was checked using the χ^2 minimization procedure ($\chi^2 = 1/(N-P) \times \sum[(I_{obs}-I_{cal}]^2/I_{obs}]$ where N is the number of data points, P the number of variable parameters, I_{obs} the observed intensity, and I_{cal} the calculated intensity).

Mössbauer spectra of natural nontronites

The initial experimental Mössbauer spectra of reference natural nontronites were reconstructed by summation of doublets reported in the published papers to fit their respective Mössbauer spectra. Experimental 298 K Mössbauer spectra of the reference natural nontronite samples were reconstructed using fitting parameters from Cardile and Johnston (1985) for Koegas (KOE), Spokane (SPO), Bingham (BIN), and Manito (MAN); from Johnston and Cardile (1985) for Garfield (GAR); from Luca (1991) for Hohen Hagen (NG-1); from Friedlander et al. (2015) for Uley (NAu-1); and from Cashion et al. (2011) for Uley (NAu-2). Experimental 77 K Mössbauer spectra of the reference natural nontronite samples were reconstructed using fitting parameters from Goodman et al. (1976) for Koegas (KOE), Garfield (GAR), Clausthal (CLA), the crocidolite deposit of Koegas (CRO), and the amosite deposit of Penge (AMO).

Model of the distribution of tetrahedral substitutions

The model of the distribution of tetrahedral substitutions was built for each sample using the Microsoft® Excel software. The model was made of three boxes representing the two tetrahedral sheets and the *tv* octahedral sheet that constitute a nontronite layer (see Figure 1 for an example). The *tv* octahedral sheet was composed of 494 octahedral sites completely

filled by Fe(III) cations, each site being represented in the Excel software by a cell. Each tetrahedral sheet was composed of 558 tetrahedral sites occupied either by Si(IV) or Fe(III) cations. The dimensions of the boxes along the *a* and *b* axes corresponded to about 135 unit cells. The construction of the tetrahedral sheets started from the center box and moved outward toward the peripheral boxes. The two tetrahedral sheets were built independently. The objective of the model was to generate a random distribution of $^{[4]}$Fe(III) cations within each tetrahedral sheet with the exclusion of the neighboring of two $^{[4]}$Fe(III) cations (i.e., Lowenstein's rule, see below for the justification of this rule). The filling of each tetrahedral sheet was done using the RAND function of Excel software. For each tetrahedron, the RAND function generated a random value, *r*, on the 0 - 1 scale, the r values for all tetrahedra being uniformly distributed between 0 and 1. Then, a logic test compared the *r* value to the *P* value, expressed on a 0 - 1 scale. The *P* value was based on the $^{[4]}$Fe(III) of the structural formula of the sample, but was adjusted to allow for Lowenstein's rule (i.e., the exclusion of the two neighboring $^{[4]}$Fe(III) - $^{[4]}$Fe(III) cations) to obtain a simulated tetrahedral sheet having a $^{[4]}$Fe(III)/ $^{[4]}$Si(IV) ratio close to that of the one of the structural formula of the sample (± 0.03). If the *r* value was higher than the *P* value, a $^{[4]}$Fe(III) cation was placed in the tetrahedron, if not, a $^{[4]}$Si(IV) was placed. For tetrahedron #1 (Figure 2), the logic test and the neighboring $^{[4]}$Fe(III) - $^{[4]}$Fe(III) exclusion could be generalized as follows:

If tetrahedron #2, and/or #3, and/or #4 is filled by a Fe(III) cation, then tetrahedron #1 will be filled by a Si(IV) cation. If not, tetrahedron #1 will be filled by a Fe(III) cation if the *r* value is greater than the *P* value or by a Si(IV) cation if the *r* value is smaller than the *P* value.

The nontronite layer was built by stacking the three modeled sheets according to the smectite structure (see for an example Figure 6). The tetrahedral environments of each $^{[6]}$Fe(III) cation (Figure 1, Table 1) was calculated using the Excel software.

One simulation corresponded to the modeling of the two tetrahedral sheets and the *tv* octahedral sheet. Two hundred simulations were performed for each sample to assess the

208 statistical results on the ratio of each local cationic tetrahedral environment around a $^{[6]}$Fe(III)
209 cation in the nontronite layer (Table 1). The $^{[4]}$Fe(III) amounts between the two tetrahedral
210 sheets of one simulation differed, at maximum, by a value of 0.12 per half unit cell, for the
211 two-hundred simulations.

212 The effect of the octahedral occupancy (i.e., *trans* or *cis* vacant octahedral sheet) on
213 the calculation of the ratio of each local cationic tetrahedral environment around a $^{[6]}$Fe(III)
214 was also evaluated. Similar results were obtained for each sample between *trans* and *cis*
215 vacant octahedral sheet simulations.

216

217 **RESULTS**

218 Mössbauer spectra of the synthetic nontronite samples at both 298 and 77 K, prior to
219 any deconvolution, exhibited a broad asymmetric doublet (Figures 3 and 4). This doublet
220 shifted slightly toward lower δ values and became more symmetric with increasing $^{[4]}$Fe(III)
221 content of the synthetic nontronite samples. No feature characteristic of Fe(II), nor any sextets
222 indicative of (oxyhydr)oxides like goethite or hematite, was observed in the Mössbauer
223 spectra of any of the synthetic nontronites at either 298 or 77 K. The Mössbauer spectra
224 recorded at 4 K (Figure 5), however, contained sextets indicating some form of magnetic
225 ordering at that low temperature. This magnetic component was already observed in natural
226 nontronites at very low temperatures or under an applied magnetic field (Cardile et al. 1986;
227 Townsend et al. 1987; Lear and Stucki 1990; Murad et al. 1990). The very high ratio of sextet
228 areas compared to the asymmetric doublet cannot be attributed to some Fe(III)
229 (oxyhydr)oxide phase here. Indeed, the magnetic component represented around 70% of the
230 iron in the sample (Table 2). If this were due to Fe(III) (oxyhydr)oxide phases, they would
231 then be the dominant phases in synthetic nontronites, which was never observed by other
232 methods (Baron et al. 2016). The deconvolution of the 4 K Mössbauer spectra evidenced a
233 range of hyperfine splitting from 34 T to a maximum value of 48 T, but with a high

proportion of a sextet having a hyperfine splitting around 40 T. This low value of hyperfine splitting did not correspond to any known (oxyhydr)oxide minerals (Table 2). Note that a high proportion of the magnetic component of the spectra was due to a broad and poorly defined sextet, suggesting a diffuse magnetic component or incomplete magnetic ordering. Consequently, the absorption spectrum of each sample was attributed to nontronite only. Despite the very high $^{[4]}$Fe(III) content of the samples, and especially of the NT6 and NT7 samples (x=1.09 and 1.3, respectively), the only obvious difference in macroscopic features of the unfitted spectra (Figures 3 and 4) was a slight change in the relative intensities of the higher velocity *vs.* the lower velocity split parts of the absorption envelope.

Empirical approach to the deconvolution of the Mössbauer spectra

Decarreau et al. (2008) fitted the 298 and 77 K Mössbauer spectra of a synthetic nontronite ($[Si_{3.25}{}^{[4]}Fe(III)_{0.75}]$ $^{[6]}Fe(III)_2O_{10}(OH)_2Na_{0.75}$) with three doublets. One of these doublets was attributed to $^{[4]}$Fe(III) and the two others to $^{[6]}$Fe(III) surrounded by [4 $^{[4]}$Si(IV)]-(3 $^{[6]}$Fe(III)) and [3 $^{[4]}$Si(IV) $^{[4]}$Fe(III)]-(3 $^{[6]}$Fe(III)). The crystal chemistry of that nontronite was very similar to the NT3 sample ($[Si_{3.25}{}^{[4]}Fe(III)_{0.77}]$ $^{[6]}Fe(III)_2O_{10}(OH)_2Na_{0.77}$) and the same three doublets were used successfully to deconvolute the NT3 Mössbauer spectrum (Figure 6), giving parameters (Table 3) similar to those found by Decarreau et al. (2008). The relative area of the doublet linked to the $^{[4]}$Fe(III) was fixed with respect to the $^{[4]}$Fe(III) content (0.77) of the NT3 sample (Table 1), and the relative area of each octahedral doublet was consistent with the crystal chemistry of the NT3 sample.

The parameters found for the three doublets of the NT3 spectra were used for the deconvolution of spectra of the NT6 sample ($[Si_{2.91}{}^{[4]}Fe(III)_{1.09}]$ $^{[6]}Fe(III)_2O_{10}(OH)_2Na_{1.09}$), which had a greater $^{[4]}$Fe(III) content than the NT3 sample. For the NT6 sample, the relative area of the doublet linked to the $^{[4]}$Fe(III) was held constant (Table 1); the parameters for the width of all doublets and the relative areas of the two doublets linked to the $^{[6]}$Fe(III) were

then allowed to float (Table 3). No correct fit was obtained with parameters of only the three NT3 doublets. As evidenced in Figure 6, the deconvolution of the NT6 spectra was clearly not possible using only the same Mössbauer parameters as those previously used for the NT3 sample.

Another approach for the deconvolution of the Mössbauer spectra

Structural constraints. On the basis of previous data (Baron et al. 2016), the synthetic nontronites had an octahedral occupancy of two per half unit cell, the two $^{[6]}$Fe(III) cations filling the two *cis* cristallographic sites (Figures 1 and 7). This is consistent with the preponderance of evidence that Fe in smectites predominantly ocupies the *cis* octahedral sites when $^{[6]}$Fe(III) content > 0.15 atoms per half unit cell (Drits et al. 2006; Wolters et al. 2009).

The octahedral Fe(III) environment of every $^{[6]}$Fe(III) cation was then the same regardless of the synthetic nontronite sample in the series, i.e., three $^{[6]}$Fe(III) neighbors. The chemical change in the synthetic series was in the $^{[4]}$Fe(III) content only, which induced changes in the composition of the neighboring tetrahedral environments of each $^{[6]}$Fe(III) cation. In the nontronite structure, each octahedral cation is linked to four neighboring tetrahedral cations (two neighbors being up and two being down, Figure 7a). Each tetrahedral cation is linked to three neighboring tetrahedral cations and to two neighboring octahedral cations (Figure 7b).

When samples (synthetic or natural) contain (i) Fe(III) and Al(III) and (ii) tetrahedral substitutions, Al(III) substitutes preferentially for Si(IV) in the tetrahedral sheet (Decarreau and Petit 2014). To assess the tetrahedral Al(III)-for-Si(IV) substitutions, Nuclear Magnetic Resonance spectroscopy (NMR) of ^{29}Si was used on 2:1 phyllosilicates (Sanz and Serratosa 1984; Herrero et al. 1985, 1987, 1989; Sanz and Robert 1992; Sanz et al. 2006). These studies demonstrated that the distribution of Al(III) atoms in the tetrahedral sheet obeys Lowenstein's rule (meaning that $^{[4]}$Al(III)-O- $^{[4]}$Al(III) linkages are avoided), and the distribution of

tetrahedral charge produced by Al(III)-for-Si(IV) substitutions is uniform (Homogeneous Dispersion of Charges (HDC) model; (Barron et al. 1985; Herrero et al. 1985, 1989; Circone et al. 1991).

In the case of Fe(III)-rich samples with low or no Al(III), as here for the synthetic nontronite samples, tetrahedral Fe(III)-for-Si(IV) substitutions occurred. The distribution of Fe(III) cations in the tetrahedral sheet cannot be measured using ^{29}Si-NMR spectroscopy due to the paramagnetic properties of Fe, so an alternative, modeling approach was used to assess the distribution of Fe(III) in the tetrahedral sheet as the $^{[4]}$Fe(III) content increased.

Model of the distribution of Fe(III) tetrahedral substitutions. The model adopted for the present study was patterned after that used by Besson et al. (1983) and Daynyak and Drits (1987). They calculated the Mössbauer parameters for natural nontronites using the Electric Field Gradient (EFG) based on the point charge model and found two doublets due to $^{[6]}$Fe(III) linked to [4Si] or [3Si-R(III)] tetrahedral environments. That model explained well the different doublets and corresponding cationic environments of $^{[6]}$Fe(III) previously observed in the Mössbauer spectra of 2:1 phyllosilicates (Goodman 1978; Besson et al. 1983; Cashion et al. 2008, 2010; Decarreau et al. 2008).

The model was based on two assumptions: (i) $^{[4]}$Fe(III) cations, as with $^{[4]}$Al(III) cations, obey Lowenstein's rule, and (ii) a uniform distribution of Fe(III)-for-Si(IV) substitutions. These assumptions were also previously made for natural and synthetic nontronite samples (Goodman 1978; Besson et al. 1983; Daynyak and Drits 1987; Decarreau et al. 2008).

From this model, three possible local cationic environments were determined for $^{[6]}$Fe(III) cations (Table 1 and Figure 7a):

(1) [4Si]-(3$^{[6]}$Fe(III))

(2) [$^{[4]}$Fe(III) 3Si]-(3$^{[6]}$Fe(III))

(3) [2[4]Fe(III) 2Si]-(3[6]Fe(III))

Only one local cationic environment was determined for [4]Fe(III) cations (Table 1 and Figure 7b):

(4) [3Si]-(2[6]Fe(III))

The presence or absence of a Na cation in the local cationic environment around a [4]Fe(III) cation was not taken into account. The proportion of each local cationic environment was then calculated for each nontronite sample (Table 1).

Deconvolution of the Mössbauer spectra of synthetic nontronites. For the deconvolution of the 298 and 77 K Mössbauer spectra, four doublets were used. They were attributed to the four local cationic environments around the Fe(III) cations determined using the distribution model (Table 1). The doublet attributed to the [4]Fe(III) cations must have a δ value lower than that of the doublets attributed to the [6]Fe(III) cations because the [4]Fe(III)-O bonds in tetrahedral coordination are more covalent than the [6]Fe(III)-O bonds in octahedral coordination. The δ values of doublets attributed to the three cationic environments around a [6]Fe(III) must be close together. The change in the local tetrahedral environment (i.e., [4Si], [[4]Fe(III) 3Si], [2[4]Fe(III) 2Si]), however, could slightly modify the geometry of the nontronite layer and consequently the geometry of the octahedral coordination of Fe(III) cations (Heller-Kallai and Rozenson 1981). The Δ values of doublets attributed to [6]Fe(III) cations must increase with the proportion of [4]Fe(III) neighboring cations as observed from EFG calculations (Besson et al. 1983; Daynyak and Drits 1987).

To fit the Mössbauer spectra at both 298 and 77 K (Figures 3 and 4, respectively), the relative area of each doublet (Table 4 and 5) was fixed using the crystal chemistry of each sample (i.e., the proportion of [4]Fe(III) and [6]Fe(III)) and the results of the distribution model of [4]Fe(III) cations of each synthetic nontronite, i.e., the proportion of each tetrahedral cationic environments of *cis* [6]Fe(III) (Table 1). The Δ values, at 298 and 77 K, were

constrained to be the same for each sample because the Δ value is not temperature dependent (Coey 1980; Dyar et al. 2008). The Mössbauer parameters were then refined separately for each spectrum to enhance the goodness of fit (Table 4 and 5).

The δ values of doublets (1), (2), and (3) at 298 and 77 K (Tables 4 and 5, respectively) were characteristic of Fe(III) cations in octahedral coordination (Coey 1980, 1984; Heller-Kallai and Rozenson 1981; Dyar 1987). The Δ values for each doublet at both 298 and 77 K (Table 4 and 5) were in agreement with the EFG calculations (Besson et al. 1983; Daynyak and Drits 1987). These authors calculated the Δ value to be in the range 0.28 - 0.35 mm s^{-1} for a $^{[6]}$Fe(III) cation surrounded by [4Si]-(3$^{[6]}$Fe(III)) and 0.6 - 0.8 mm s^{-1} for a $^{[6]}$Fe(III) cation surrounded by [$^{[4]}$R(III) 3Si]-(3$^{[6]}$R(III)). The Δ value corresponding to the local cationic environment [2$^{[4]}$Fe(III) 2Si]-(3$^{[6]}$Fe(III)) surrounding a $^{[6]}$Fe(III) cation was not calculated by Daynyak and Drits (1987), but the large increase in the value of Δ observed when a Fe(III)-for-Si substitution occurs suggested that an additional tetrahedral substitution around a $^{[6]}$Fe(III) cation should yield a Δ value > 0.8 mm s^{-1}. The value for Δ obtained from the curve fitting here was consistent with that prediction, being between 1.09 and 1.27 mm s^{-1} for the [2$^{[4]}$Fe(III) 2Si]-(3$^{[6]}$Fe(III)) configuration around a $^{[6]}$Fe(III) cation (Table 4 and 5).

The low δ values of doublet (4) (Table 4 and 5) were characteristic of Fe(III) cations in tetrahedral coordination in natural and synthetic nontronites (Goodman et al. 1976; Goodman 1978; Coey 1980, 1984; Besson et al. 1983; Daynyak and Drits 1987; Luca 1991). The Δ values of doublet (4) were also similar to those reported for nontronite samples (Goodman et al. 1976; Goodman 1978; Coey 1984; Decarreau et al. 2008).

Application to natural nontronites from the literature.

The method for deconvolution of Mössbauer spectra developed for synthetic nontronites was then applied to reference natural nontronites. The reconstructed experimental

Mössbauer spectra were then refitted using four doublets as described here for the synthetic nontronites, using Mössbauer parameters according to their recording temperature.

This approach was first applied to the Koegas (KOE) nontronite spectrum (Figure 8) which had a crystal chemistry similar to the one of synthetic nontronites: high Fe(III) content and low Al and Mg contents (Table 6). The proportion of each local cationic environment around a $^{[6]}$Fe(III) cation was calculated using the model for the distribution of tetrahedral substitutions as described above for synthetic nontronites, with a total extent of tetrahedral substitutions ($^{[4]}$Fe(III) and $^{[4]}$Al) of 0.7 per half unit cell. No distinction was made between $^{[4]}$Fe(III) and $^{[4]}$Al for the calculation of the proportion of each local tetrahedral environment around a $^{[6]}$Fe(III) cation. Also assumed was that vvery low $^{[6]}$Al and $^{[6]}$Mg contents did not lead to detectable Mössbauer features. The deconvolution was then performed with the additional constraint that the relative area of each of the four doublets was the same for spectra recorded at 298 and 77 K (Tables 7 and 8).

The Mössbauer spectra of the Garfield nontronite (GAR) (Figure 8) with a larger $^{[4]}$Al content (Manceau et al. 2000; Gates et al. 2002) were deconvoluted to test the assumption that the effects of $^{[4]}$Al and $^{[4]}$Fe(III) subsitutions on Mössbauer parameters are identical. The resulting parameters for Garfield nontronite (having a large $^{[4]}$Al content) were similar to those of the Koegas nontronite (having a large $^{[4]}$Fe(III) content) (Tables 7 and 8), indicating that tetrahedral substitutions by Fe(III) and Al have similar effects on the $^{[6]}$Fe(III) Mössbauer parameters.

Six other 298 K Mössbauer spectra and three other 77 K Mössbauer spectra of reference natural nontronites (Table 6) were selected and deconvoluted using the same procedure as for the Koegas and the Garfield nontronites (Figure 9 and 10; Tables 7 and 8). Good fits of all Mössbauer spectra of reference natural nontronites were obtained using only four doublets The amounts of Mg being always very low (Tables 7 and 8) in these natural nontronites, the $^{[6]}$Fe(III) surrounded by (2$^{[6]}$Fe(III) $^{[6]}$Mg) was too low to be detectable.

Note that for the natural sample NAu-2, Cashion et al. (2011) showed that 92% of the Mössbauer spectrum only could be attributed to known strutural iron features in nontronite layers. The remaining 8% corresponded to a doublet having a large Δ (1.28 mm s^{-1}), easily distinguishable with extra features compared to other samples (Figure 9). Using the procedure described above for the deconvolution of Mössbauer spectra, the inconsistency in the Mössbauer parameters found is in accordance with the occurrence of external iron (interlayer Fe(III) or impurity or Fe-pillaring) as concluded by Cashion et al. (2011). Then, the deconvolution of the 298 K Mössbauer spectra of the NAu-2 sample was done using an extra doublet with the fixed parameters of Cashion et al. (2011) (i.e., δ = 0.41 mm s^{-1}, Δ = 1.28 mm s^{-1}, width = 0.26 mm s^{-1}, and area = 8%).

DISCUSSION

The Mössbauer parameters from the four doublets used to fit the spectra obtained at both 298 and 77 K for all synthetic nontronite samples were distributed among eight clusters of δ *vs.* Δ (Figure 11; values in Tables 4 and 5), confirming the self consistency of the fitting model. The δ values of the doublets attributed to the three local tetrahedral cationic environments around a $^{[6]}$Fe(III) were similar regardless of the sample, and were in the 0.32 – 0.35 mm s^{-1} range at 298 K and in the 0.44 – 0.47 mm s^{-1} range at 77 K. This small variability in the δ value suggested that the different tetrahedral environments surrounding the $^{[6]}$Fe(III) cation had only a small effect on the covalence of bonds between the $^{[6]}$Fe(III) cation and the neighboring oxygen ions. The width of these three doublets was in the 0.36 – 0.49 mm s^{-1} range for all samples, whether at 298 or 77 K. The Δ values at 298 K and 77 K were in the 0.32 – 0.46 mm s^{-1}, 0.63 – 0.84 mm s^{-1}, and 1.09 – 1.27 mm s^{-1} ranges for the [4Si]-(3$^{[6]}$Fe(III)), [$^{[4]}$Fe(III) 3Si^{4+}]-(3$^{[6]}$Fe(III)), and [2$^{[4]}$Fe(III) 2Si^{4+}]-(3$^{[6]}$Fe(III)) cationic environments of $^{[6]}$Fe(III), respectively (Tables 4 and 5). This increase in Δ was linked to the

414 increase in EFG produced by tetrahedral Fe(III)-for-Si substitutions occurring around a
415 $^{[6]}$Fe(III) cation.

416 A high variability was observed, however, in Δ values for the same local tetrahedral
417 cationic environment across samples NT0 to NT7 (Table 4 and 5). These samples differed not
418 only in their tetrahedral Fe(III) content, but also in their crystallinity. The Δ values of the
419 different local tetrahedral cationic environments around a $^{[6]}$Fe(III) correlated well with the
420 full width at half maximum (FWHM) values of the *(06-33)* reflection of XRD patterns of the
421 same sample (the FWHM was measured using XRD data from Baron et al. 2016) (Figure 12).
422 The FWHM of the d*(06-33)* is linked to the crystal coherent scattering domain size (CSDS) of
423 samples in the *(ab)* plane (Moore and Reynolds 1997), i.e., their in-plane "crystallinity," a
424 decrease in the FWHM corresponds to an increase in sample crystallinity. These correlations
425 (Figure 12) are evidence of the influence of crystallinity on the Δ values.

426 Nontronite particles could be considered as containing two types of crystallographic
427 sites, namely, those located inside the coherent crystal domains and those on the border of
428 coherent crystal domains. The border sites are well known to be more distorted than those of
429 the central domain sites, and the smaller the crystal coherent domain size (i.e., low
430 crystallinity), the larger the ratio of border to heart sites. Distortion of crystallographic sites is
431 well known to increase the Δ values (Dyar et al. 2006). When the crystallinity of samples was
432 low, the correspondingly larger ratio of distorted border sites could induce an increase in Δ
433 values. Similarly, Friedlander et al. (2015) obtained Mössbauer spectra of natural nontronite
434 before and after experimental impacts (meteor simulated impacts) between 10 and 40 GPa,
435 showing that impacts produced structural deformations (i.e., disordered crystallographic sites)
436 that resulted in an increase in Δ values. The degree of crystallinity of nontronite samples
437 could affect the Δ values of doublets. The Mössbauer spectra of synthetic nontronites were
438 much broader than those of natural nontronites (compare Figures 3 and 4 with Figures 8, 9,

439 and 10), consistent with the preceding discussion that Δ values increase with a decrease in
440 sample crystallinity, given that synthetic nontronites are less crystalline than natural ones.

441 The Δ and width values of the doublet assigned to $^{[4]}$Fe(III) were similar for all
442 synthetic samples and were in the range of 0.59 – 0.64 mm s^{-1} and 0.39 – 0.45 mm s^{-1},
443 respectively (Tables 4 and 5). The δ values were in the range of 0.16 – 0.2 mm s^{-1} and 0.26 –
444 0.3 mm s^{-1} for 298 and 77 K, respectively. The low variability in Δ for the $^{[4]}$Fe(III) doublets
445 compared to the $^{[6]}$Fe(III) doublets for synthetic nontronites (Figure 11) is consistent with the
446 much lower capability of the tetrahedral sites to distort compared with the octahedral sites
447 (Manceau et al. 1998), the tetrahedron being able to rotate and tilt to match the tetrahedral
448 sheets with the octahedral sheet of a layer.

449 These deconvolutions of the Mössbauer spectra of the synthetic nontronite series, with
450 parameters consistent with literature values, strongly argued that the distribution of $^{[4]}$Fe(III)
451 cations was uniform and follows the Lowenstein's law. This approach to deconvolution,
452 taking into account the crystal chemistry of samples and introducing structural constraints to
453 guide the process, yielded robust parameters for each of the local environments around a
454 Fe(III) cation in the nontronite structure.

455 The Δ values obtained for natural nontronite spectra were less than those determined
456 for synthetic nontronites (Tables 7 and 8), suggesting a population of crystallographic sites
457 with a smaller mean square displacement of the local crystal symmetry in natural nontronites
458 than in synthetic nontronites (Dyar et al. 2006; Friedlander et al. 2015). Indeed, the crystal
459 size coherency of the natural nontronites is greater than that of synthetic nontronites. This
460 trend clearly exemplified how the sample crystallinity can modify the Δ values for natural and
461 synthetic nontronites.

462 The δ values determined for both $^{[4]}$Fe(III) and $^{[6]}$Fe(III) doublets of natural nontronites
463 were slightly greater (around 0.04 mm s^{-1}) than those determined for the synthetic nontronites
464 (Table 7). This difference, however, possibly could have arisen from different calibrations of

the spectrometers used for the natural samples compared to the synthetic samples and may not be a true distinguishing feature.

The atomic percentages (at.%) of $^{[4]}$Fe(III) relative to total Fe(III) estimated using the present deconvolutions of the Mössbauer spectra of natural nontronite samples were compared with results from the original deconvolutions (Goodman et al. 1976; Cardile and Johnston 1985; Johnston and Cardile 1985; Luca 1991; Friedlander et al. 2015), from X-ray absorption spectroscopy (Manceau et al. 2000; Gates et al. 2002), and from calculations of Al(III)/Fe(III) distribution using a partition coefficient $Kd_{[4]/[6]}$ of 0.006 (Decarreau and Petit 2014) (Table 9). The $^{[4]}$Fe(III) contents estimated in the present work were in good agreement with the $^{[4]}$Fe(III) contents calculated using the partition coefficient $Kd_{[4]/[6]}$ except for the NG-1 nontronite sample. However, the NG-1 sample seems to be heterogeneous, as suggested by structural formulae being given by different authors (Schneiderhöhn 1965; Köster et al. 1999; Manceau et al. 2000). The $^{[4]}$Fe(III) content obtained using the partition coefficient $Kd_{[4]/[6]}$ varied from 1 to 6% depending on the structural formula used. The amount of $^{[4]}$Fe(III) for the NG-1 nontronite sample estimated in the present study agreed with the results found using X-ray absorption spectroscopy (Manceau et al. 2000; Gates et al. 2002). For the other nontronite samples, the estimated $^{[4]}$Fe(III) contents were in agreement with the results of Gates et al. (2002) in spite of the general overestimation of the $^{[4]}$Fe(III) content using X-ray absorption spectroscopy.

The detection of low or very low $^{[4]}$Fe(III) content (< 5% of the total Fe(III) amount) was difficult using the present deconvolution process (e.g., samples GAR, MAN, NAu-1, NAu-2, and BIN). For the asymmetric spectra of GAR and NAu-2, for example, a measurable amount of $^{[4]}$Fe(III) was detected. For the three other nontronites, estimation of the true value of $^{[4]}$Fe(III) from Mössbauer spectra was not possible.

IMPLICATIONS

Mössbauer spectroscopy has often been used to determine the Fe(III)/Fe(II) ratio and the distribution of Fe(III) between the octahedral and the tetrahedral sheets of minerals with unknown crystal chemistry. The iron status of clay minerals was obtained by fitting the Mössbauer spectra by a sum of doublets.

The originality in the present paper was to do the reverse, i.e., to use a series of synthetic nontronites with a wide range of $^{[4]}$Fe(III) contents and a known crystal chemistry previously determined (Baron et al., 2016) to study Mössbauer spectra of nontronites. The synthetic nontronites have the advantage of containing only Si, Fe(III), Na, O, and H in their structure, thus simplifying the constraints needed to carry out the deconvolution and especially the interpretation of the Mössbauer spectra. A second originality of the present paper has been to model the structure of the synthetic samples from their known crystal chemistry. This structural model defined the allowed proportions of all cationic environments for each sample of the series.

The deconvolution of Mössbauer spectra of synthetic samples was done by fixing the area of doublets for each cationic environment from the results of the structural model. This fundamental step allowed a more proper interpretation of the Mössbauer spectra and a complete and coherent representation of the distribution of Fe(III) between the octahedral and tetrahedral crystallographic sites of the nontronite structure. Although the use of a simple model from a sum of Lorentzian line shape has been considered to be less theoritically correct than a Voigt-based model (Rancourt 1994), the self-consistent results obtained with the synthetic nontronites provided evidence of the important role of the local environment around a $^{[6]}$Fe(III) cation, as well as the role of crystallinity (i.e., the long distance lattice defects), in determining the Mössbauer parameter values, particularly the value for Δ. As previously mentioned by Rancourt (1994), the empirical deconvolution of Mössbauer spectra did not tend to a unique solution. In the present paper, however, the use of six synthetic nontronite

samples in which Mössbauer parameters at both 77 K and 298 K tended toward similar and coherent δ and Δ values engendered confidence in the methodology. This paper provided, in that sense, robust values of Mössbauer parameters of $^{[4]}$Fe(III) and $^{[6]}$Fe(III) in clay mineral structures.

Some guiding principles for using Mössbauer spectroscopy can be extracted from this study. First, the deconvolution of Mössbauer spectra of clay minerals should take into account, as much as possible, the whole Fe(III) environment and should rely on the use of a crystal chemistry model. In particular, the tetrahedral environment of the $^{[6]}$Fe(III) atoms must be taken into account. Second, Mössbauer spectroscopy should not be used alone to deduce the crystal chemistry of Fe-rich clay minerals. The results of the present study on Mg- and Al-poor natural samples tends to show that $^{[6]}$Mg does not produce a significant modification of the Mössbauer parameters and that Al(III) and Fe(III) have the same effect on Mössbauer spectra of clay minerals as previously shown by Drits et al. (1992). Nevertheless, for smectites having a high $^{[6]}$Mg content, further doublets would be needed to take into account all the $^{[6]}$Fe(III) environments, both in the octahedral and tetrahedral sheets. Other spectroscopies, and infrared spectroscopy in particular, remain more versatile and appropriate techniques to obtain crystal-chemical information on octahedral occupancies of clay minerals (e.g., Petit et al. 2006).

Although the method developed in the present paper was not physics based (approximate line shapes, f recoil was not known, etc.) it allows for mineralogists to interpret Mössbauer spectra of nontronites (and potentially others Fe(III)-rich clay minerals) and to obtain a quantitative $^{[4]}$Fe(III)/$^{[6]}$Fe(III) ratio. For nontronite samples with a low or very low $^{[4]}$Fe(III) content (< 5% of the total Fe(III)), however, the quantification of $^{[4]}$Fe(III) was only qualitative.

REFERENCES

Annersten, H., Devanarayanan, S., Häggström, L., and Wäppling, R. (1971) Mössbauer study of synthetic ferriphlogopite $KMg_3Fe^{3+}Si_3O_{10}(OH)_2$. Physica Status Solidi (B), 48, 137–138.

Baron, F., Petit, S., Tertre, E., and Decarreau, A. (2016) Influence of aqueous Si and Fe speciation on tetrahedral Fe(III) substitutions in nontronites: a clay synthesis approach. Clays and Clay Minerals, 64, 230.

Barron, P.F., Slade, P., and Frost, R.L. (1985) Ordering of aluminum in tetrahedral sites in mixed-layer 2:1 phyllosilicates by solid-state high-resolution NMR. The Journal of Physical Chemistry, 89, 3880–3885.

Besson, G., Bookin, A.S., Dainyak, L.G., Rautureau, M., Tsipursky, S.I., Tchoubar, C., and Drits, V.A. (1983) Use of diffraction and Mössbauer methods for the structural and crystallochemical characterization of nontronites. Journal of Applied Crystallography, 16, 374–383.

Bonnin, D., Calas, G., Suquet, H., and Pezerat, H. (1985) Sites occupancy of Fe_{3+} in Garfield Nontronite: A spectroscopic study. Physics and Chemistry of Minerals, 12, 55–64.

Cardile, C.M. (1989) Tetrahedral iron in smectite; a critical comment. Clays and Clay Minerals, 37, 185–188.

Cardile, C.M., and Johnston, J.H. (1985) Structural studies of nontronites with different iron contents by ^{57}Fe Mössbauer spectroscopy. Clays and Clay Minerals, 33, 295–300.

Cardile, C.M., Johnson, J.H., and Dickson, D.P.E. (1986) Magnetic ordering at 4.2 and 1.3 K in nontronites of different iron contents; a ^{57}Fe Mössbauer spectroscopic study. Clays and Clay Minerals, 34, 233–238.

Cashion, J.D., Gates, W.P., and Thomson, A. (2008) Mössbauer and IR analysis of iron sites in four ferruginous smectites. Clay Minerals, 43, 83–93.

Cashion, J.D., Gates, W.P., and Riley, G.M. (2010) Origin of the two quadrupole doublets in NAu-1 nontronite. Journal of Physics: Conference Series, 217, 012065.

Cashion, J.D.,Gates, W.P., Greaves, T.L. and Dorjkhaidav, O. (2011) Identification of Fe^{3+} site coordinations in Nau-2 Nontronite, Proc. 35th A&NZ Condensed Matter and Materials Meeting, Wagga Wagga, Australia.

Circone, S., Navrotsky, A., Kirkpatrick, R.J., and Graham, C.M. (1991) Substitution of super $^{[6,4]}$Al in phlogopite; mica characterization, unit-cell variation, ^{27}Al and ^{29}Si MAS-NMR spectroscopy, and Al-Si distribution in the tetrahedral sheet. American Mineralogist, 76, 1485–1501.

Coey, J.M.D. (1980) Clay minerals and their transformations studied with nuclear techniques: the contribution of Mössbauer spectroscopy. Atomic Energy Review, 18, 73–124.

——— (1984) Mössbauer spectroscopy of silicate minerals. In G.J. Long, Ed., Mössbauer spectroscopy applied to inorganic chemistry Vol. 1, pp. 443–509. New York.

581 Daynyak, L.G., and Drits, V.A. (1987) Interpretation of Mössbauer spectra of nontronite,
582 celadonite, and glauconite. Clays and Clay Minerals, 35, 363–372.

583 Decarreau, A., and Petit, S. (2014) Fe^{3+}/Al^{3+} partitioning between tetrahedral and octahedral
584 sites in dioctahedral smectites. Clay Minerals, 49, 657–665.

585 Decarreau, A., Petit, S., Martin, F., Farges, F., Vieillard, P., and Joussein, E. (2008)
586 Hydrothermal synthesis, between 75 and 150°C, of high-charge, ferric nontronites.
587 Clays and Clay Minerals, 56, 322–337.

588 De Grave, E., and Van Alboom, A. (1991) Evaluation of ferrous and ferric Mössbauer
589 fractions. Physics and Chemistry of Minerals, 18, 337–342.

590 Drits, V.A., McCarty, D.K., and Zviagina, B.B. (2006) Crystal-chemical factors responsible
591 for the distribution of octahedral cations over trans- and cis-sites in dioctahedral 2:1
592 layer silicates. Clays and Clay Minerals, 54, 131–152.

593 Dyar, M.D. (1987) A review of Mössbauer data on trioctahedral micas; evidence for
594 tetrahedral Fe^{3+} and cation ordering. American Mineralogist, 72, 102–112.

595 ——— (1993) Mössbauer spectroscopy of tetrahedral Fe^{3+} in trioctahedral micas; discussion.
596 American Mineralogist, 78, 665–668.

597 Dyar, M.D., and Schaefer, M.W. (2008) Discriminating among layer silicates using remote
598 Mössbauer spectroscopy. Martian Phyllosilicates: Recorders of aqueous processes,
599 LPI abstract.

600 Dyar, M.D., Agresti, D.G., Schaefer, M.W., Grant, C.A., and Sklute, E.C. (2006) Mössbauer
601 spectroscopy of Earth and planetary materials. Annual Review of Earth and Planetary
602 Sciences, 34, 83–125.

603 Dyar, M.D., Schaefer, M.W., Sklute, E.C., and Bishop, J.L. (2008) Mössbauer spectroscopy
604 of phyllosilicates: effects of fitting models on recoil-free fractions and redox ratios.
605 Clay Minerals, 43, 3–33.

606 Friedlander, L.R., Glotch, T.D., Bish, D.L., Darby Dyar, M., Sharp, T.G., Sklute, E.C., and
607 Michalski, J.R. (2015) Structural and spectroscopic changes to natural nontronite
608 induced by experimental impacts between 10 and 40 GPa. Journal of Geophysical
609 Research: Planets, 120, 888–912.

610 Gates, W.P., Slade, P.G., Manceau, A., and Lanson, B. (2002) Site occupancies by iron in
611 nontronites. Clays and Clay Minerals, 50, 223–239.

612 Goodman, B.A. (1978) The Mössbauer spectra of nontronites; consideration of an alternative
613 assignment. Clays and Clay Minerals, 26, 176–177.

614 Goodman, B.A., Russell, J.D., Fraser, A.R., and Woodhams, F.W.D. (1976) A Mössbauer and
615 I.R. spectroscopic study of the structure of nontronite. Clays and Clay Minerals, 24,
616 53–59.

617 Heller-Kallai, L., and Rozenson, I. (1981) The use of Mössbauer spectroscopy of iron in clay
618 mineralogy. Physics and Chemistry of Minerals, 7, 223–238.

Herrero, C.P., Sanz, J., and Serratosa, J.M. (1985) Tetrahedral cation ordering in layer silicates by ^{29}Si NMR spectroscopy. Solid State Communications, 53, 151–154.

Herrero, C.P., Gregorkiewitz, M., Sanz, J., and Serratosa, J.M. (1987) ^{29}Si MAS-NMR spectroscopy of mica-type silicates: Observed and predicted distribution of tetrahedral Al-Si. Physics and Chemistry of Minerals, 15, 84–90.

Herrero, C.P., Sanz, J., and Serratosa, J.M. (1989) Dispersion of charge deficits in a tetrahedral sheet of phyllosilicates: analysis from ^{29}Si NMR spectra. The Journal of Physical Chemistry, 93, 4311–4315.

Johnston, J.H., and Cardile, C.M. (1985) Iron sites in nontronite and the effect of interlayer cations from Mössbauer spectra. Clays and Clay Minerals, 33, 21–30.

Klingelhöfer, G., Morris, R.V., Bernhardt, B., Schröder, C., Rodionov, D.S., de Souza, P.A., Yen, A., Gellert, R., Evlanov, E.N., Zubkov, B., and others (2004) Jarosite and Hematite at Meridiani Planum from Opportunity's Mössbauer Spectrometer. Science, 306, 1740–1745.

Klingelhöfer, G., DeGrave, E., Morris, R.V., Alboom, A., Resende, V.G., Souza, P.A., Rodionov, D., Schröder, C., Ming, D.W., and Yen, A. (2006) Mössbauer spectroscopy on Mars: goethite in the Columbia Hills at Gusev crater. Hyperfine Interactions, 166, 549–554.

Köster, H.M., Ehrlicher, U., Gilg, H.A., Jordan, R., Murad, E., and Onnich, K. (1999) Mineralogical and chemical characteristics of five nontronites and Fe-rich smectites. Clay Minerals, 34, 579–599.

Lear, P.R., and Stucki, J.W. (1990) Magnetic properties and site occupancy of iron in nontronite. Clay Minerals, 25, 3–13.

Luca, V. (1991) Detection of tetrahedral Fe^{3+} sites in nontronite and vermiculite by Mössbauer spectroscopy. Clays and Clay Minerals, 39, 467–477.

Manceau, A., Chateigner, D., and Gates, W.P. (1998) Polarized EXAFS, distance-valence least-squares modeling (DVLS), and quantitative texture analysis approaches to the structural refinement of Garfield nontronite. Physics and Chemistry of Minerals, 25, 347–365.

Manceau, A., Lanson, B., Drits, V.A., Chateigner, D., Gates, W.P., Wu, J., Huo, D., and Stucki, J.W. (2000) Oxidation-reduction mechanism of iron in dioctahedral smectites: I. Crystal chemistry of oxidized reference nontronites. American Mineralogist, 85, 133–152.

Moore, D.M., and Reynolds, R.C. (1997) X-Ray Diffraction and the identification and analysis of Clay Minerals, Oxford University Press., 378 p. Oxford.

Morris, R.V., Klingelhöfer, G., Bernhardt, B., Schröder, C., Rodionov, D.S., de Souza, P.A., Yen, A., Gellert, R., Evlanov, E.N., Foh, J., and others (2004) Mineralogy at Gusev Crater from the Mössbauer Spectrometer on the Spirit Rover. Science, 305, 833–836.

Murad, E. (2008) ^{57}Fe Mössbauer spectroscopy: a tool for the remote characterization of phyllosilicates? Martian Phyllosilicates: Recorders of aqueous processes, LPI abstract.

——— (2013) Mössbauer Spectroscopy. In F. Bergaya and G. Lagaly, Eds., Handbook of Clay Science pp. 11–24. Elsevier, Amsterdam.

Murad, E., and Cashion, J. (2004) Mössbauer spectroscopy of environmental materials and their industrial utilization. Springer Science & Business Media.

Murad, E., Cashion, J.D., and Brown, L.J. (1990) Magnetic ordering in Garfield nontronite under applied magnetic fields. Clay Minerals, 25, 261–269.

Petit, S. (2006) Fourier Transform Infrared Spectroscopy, In Bergaya, F. and Lagaly, G. Eds., Handbook of Clay Science, p. 909–918. Elsevier, Amsterdam.

Petit, S., Prot, T., Decarreau, A., Mosser, C., and Toledo-Groke, M.C. (1992) Crystallochemical study of a population of particles in smectites from a lateritic weathering profile. Clays and Clay Minerals, 40, 436–445.

Petit, S., Decarreau, A., Gates, W., Andrieux, P., and Grauby, O. (2015) Hydrothermal synthesis of dioctahedral smectites: The Al–Fe^{3+} chemical series. Part II: Crystal-chemistry. Applied Clay Science, 104, 96–105.

Rancourt, D.G. (1993) Mössbauer spectroscopy of tetrahedral Fe^{3+} in trioctahedral micas; reply. American Mineralogist, 78, 669–671.

——— (1994) Mössbauer spectroscopy of minerals: I. Inadequacy of Lorentzian-line doublets in fitting spectra arising from quadrupole splitting distributions. Physics and Chemistry of Minerals, 21, 244–249.

Rozenson, I., and Heller-Kallai, L. (1977) Mossbauer spectra of dioctahedral smectites. Clays and Clay Minerals, 25, 94–101.

Sanz, J., and Robert, J.-L. (1992) Influence of structural factors on ^{29}Si and ^{27}Al NMR chemical shifts of phyllosilicates 2:1. Physics and Chemistry of Minerals, 19, 39–45.

Sanz, J., and Serratosa, J.M. (1984) ^{29}Si and ^{27}Al high-resolution MAS-NMR spectra of phyllosilicates. Journal of the American Chemical Society, 106, 4790–4793.

Sanz, J., Robert, J.-L., Diaz, M., and Sobrados, I. (2006) Influence of charge location on ^{29}Si NMR chemical shift of 2:1 phyllosilicates. American Mineralogist, 91, 544–550.

Schneiderhöhn, P. (1965) Nontronit vom Hohen Hagen und Chloropal vom Meenser Steinberg bei Göttingen. Tschermaks mineralogische und petrographische Mitteilungen, 10, 385–399.

Schröder, C., Klingelhöfer, G., Morris, R.V., Bernhardt, B., Blumers, M., Fleischer, I., Rodionov, D.S., López, J.G., and de Souza, P.A. (2011) Field-portable Mössbauer spectroscopy on Earth, the Moon, Mars, and beyond. Geochemistry: Exploration, Environment, Analysis, 11, 129–143.

Schwertmann, U., and Cornell, R.M. (1991) Iron oxides in the laboratory, VCH. Weinheim, Germany.

Stucki, J.W. (2013) Properties and behaviour of iron in clay minerals. In F. Bergaya and G. Lagaly, Eds., Handbook of Clay Science pp. 559–612. Elsevier, Amsterdam.

697 Stucki, J.W., Su, K., Pentráková, L., and Pentrák, M. (2014) Methods for handling redox-
698 sensitive smectite dispersions. Clay Minerals, 49, 359–377.

699 Townsend, M.G., Longworth, G., Ross, C.A.M., and Provencher, R. (1987) Ferromagnetic or
700 antiferromagnetic Fe III spin configurations in sheet silicates. Physics and Chemistry
701 of Minerals, 15, 64–70.

702 Wolters, F., Lagaly, G., Kahr, G., Nueesch, R., and Emmerich, K. (2009) A comprehensive
703 characterization of dioctahedral smectites. Clays and Clay Minerals, 57, 115–133.

704

This is a preprint, the final version is subject to change, of the American Mineralogist (MSA)
Cite as Authors (Year) Title. American Mineralogist, in press.
(DOI will not work until issue is live.) DOI: http://dx.doi.org/10.2138/am-2017-6039

Table 1: Crystal chemistry of the synthetic nontronites.

			Proportion of the local cationic environments around a Fe(III) (%)			
			$^{[6]}$Fe(III)			$^{[4]}$Fe(III)
Sample	x	FWHM d*(06-33)* (°2θ)	[4Si]-($3^{[6]}$Fe(III))	[$^{[4]}$Fe(III) 3Si]-($3^{[6]}$Fe(III))	[$2^{[4]}$Fe(III) 2Si]-($3^{[6]}$Fe(III))	[3Si]-($2^{[6]}$Fe(III))
NT0	0.51	1.576	45.0 ± 2.2	30.0 ± 2.1	4.9 ± 1.0	20.1 ± 1.0
NT1	0.57	1.589	39.6 ± 2.1	31.6 ± 2.0	6.4 ± 1.1	22.4 ± 1.0
NT3	0.78	1.466	26.8 ± 1.8	34.1 ± 1.9	10.2 ± 1.2	28.2 ± 0.8
NT5	0.99	1.039	17.2 ± 1.3	33.0 ± 1.6	16.5 ± 1.3	33.3 ± 0.7
NT6	1.09	1.155	13.5 ± 1.2	31.8 ± 1.6	19.2 ± 1.2	35.4 ± 0.6
NT7	1.3	1.050	7.7 ± 1.0	27.54 ± 1.5	25.4 ± 1.4	39.4 ± 0.6

Note(s): x: $^{[4]}$Fe(III) contents on the basis of $[Si_{4-x}{}^{[4]}Fe(III)_x]\,{}^{[6]}Fe(III)_2O_{10}(OH)_2Na_x$ structural formula; FWHM: full width at half maximum of the XRD (06-33) reflection (Data from Baron et al., 2016); Proportions (in at.% of total Fe(III)) of each local cationic environments neighboring a Fe(III) cation within the nontronite sample obtained using the model of distribution of tetrahedral substitutions (See text). The uncertainty in the proportion of the local cationic environments was determined using two hundred simulations.

Table 2: Ranges of magnetic hyperfine fields in Mössbauer spectra of synthetic nontronites and natural Fe (oxyhydr)oxide samples.

	Hyperfine splitting range (T)	**Magnetic area (%)**	**Part of diffuse magnetism area (%)**
NT0	35 - 47	75	43
NT1	34 - 46	61	36
NT3	37 - 48	65	35
NT5	35 - 46	79	44
NT6	34 - 45	75	31
NT7	35 - 45	73	39
Hematite	54.2[a]		
Goethite	50.6 [a]		
Ferrihydrite	47 - 50 [a]		

[a] *corresponds to data from (Schwertmann and Cornell 1991)*

Table 3: Mössbauer parameters of the NT3 and NT6 synthetic nontronite spectra using three doublets.

		NT3		NT6	
		298 K	**77 K**	**298 K**	**77 K**
Doublet (1) Tetrahedral	δ (mm s^{-1})	0.16	0.18	0.16	0.19
	Δ (mm s^{-1})	0.60	0.63	0.62	0.65
	Width (mm s^{-1})	0.42	0.40	0.44	0.42
	Area (%)	27.9 [a]	28.3 [a]	35.0 [a]	35.0 [a]
Doublet (2) Octahedral	δ (mm s^{-1})	0.35	0.41	0.36	0.43
	Δ (mm s^{-1})	0.70	0.71	0.72	0.73
	Width (mm s^{-1})	0.49	0.48	0.51	0.50
	Area (%)	56.3	56.0	65.0	65.0
Doublet (3) Octahedral	δ (mm s^{-1})	0.33	0.41	0.35	0.43
	Δ (mm s^{-1})	0.38	0.38	0.40	0.40
	Width (mm s^{-1})	0.34	0.32	0.32	0.30
	Area (%)	15.8	15.7	0.00	0.00
	χ^2	1.10	2.74	2.64	4.95

Note(s): Doublets 1, 2, and 3 correspond to doublets in the Figure 6. [a]: constrained parameter (± 5% of the theoretical area value of tetrahedral doublets determined from the structural formula).

This is a preprint, the final version is subject to change, of the American Mineralogist (MSA)
Cite as Authors (Year) Title. American Mineralogist, in press.
(DOI will not work until issue is live.) DOI: http://dx.doi.org/10.2138/am-2017-6039

Table 4: Mössbauer parameters of the 298 K Mössbauer spectra of the synthetic nontronites using four doublets.

		NT7	NT6	NT5	NT3	NT1	NT0
Doublet (1) Octahedral $[4Si^{4+}]$-$(3^{VI}Fe^{3+})$	δ (mm s^{-1})	0.35	0.32	0.34	0.34	0.34	0.34
	Δ (mm s^{-1})	0.34	0.41	0.36	0.35	0.42	0.46
	Width (mm s^{-1})	0.36	0.44	0.41	0.42	0.44	0.48
	Area (%)	7.3 [a]	13.4 [a]	17.1 [a]	26.9 [a]	39.7 [a]	44.8 [a]
Doublet (2) Octahedral $[^{IV}Fe^{3+}\ 3Si^{4+}]$-$(3^{VI}Fe^{3+})$	δ (mm s^{-1})	0.35	0.32	0.34	0.34	0.34	0.34
	Δ (mm s^{-1})	0.64	0.70	0.67	0.67	0.74	0.84
	Width (mm s^{-1})	0.36	0.38	0.39	0.36	0.41	0.45
	Area (%)	28.6 [a]	31.7 [a]	32.8 [a]	34.0 [a]	31.4 [a]	30.2 [a]
Doublet (3) Octahedral $[2^{IV}Fe^{3+}\ 2Si^{4+}]$-$(3^{VI}Fe^{3+})$	δ (mm s^{-1})	0.32	0.32	0.34	0.35	0.35	0.35
	Δ (mm s^{-1})	1.13	1.16	1.09	1.17	1.21	1.27
	Width (mm s^{-1})	0.41	0.46	0.49	0.37	0.39	0.39
	Area (%)	24.7 [a]	19.3 [a]	16.6 [a]	10.9 [a]	6.4 [a]	4.9 [a]
Doublet (4) Tetrahedral $[3Si^{4+}]$-$(2^{VI}Fe^{3+})$	δ (mm s^{-1})	0.20	0.20	0.18	0.18	0.16	0.16
	Δ (mm s^{-1})	0.59	0.64	0.60	0.60	0.60	0.60
	Width (mm s^{-1})	0.42	0.45	0.46	0.40	0.39	0.40
	Area (%)	39.3 [a]	35.6 [a]	33.4 [a]	28.3 [a]	22.5 [a]	20.2 [a]
χ^2		1.25	0.75	0.63	1.05	0.70	0.76

[a]*: constrained parameter (± 5% of the theoretical area value of doublets determined from the structural model).*

This is a preprint, the final version is subject to change, of the American Mineralogist (MSA)
Cite as Authors (Year) Title. American Mineralogist, in press.
(DOI will not work until issue is live.) DOI: http://dx.doi.org/10.2138/am-2017-6039

Table 5: Mössbauer parameters of the 77 K Mössbauer spectra of the synthetic nontronites using four doublets.

		NT7	NT6	NT5	NT3	NT1	NT0
Doublet (1) Octahedral $[4Si^{4+}]$-$(3^{VI}Fe^{3+})$	δ (mm s^{-1})	0.47	0.47	0.47	0.46	0.45	0.45
	Δ (mm s^{-1})	0.32	0.41	0.37	0.37	0.41	0.45
	Width (mm s^{-1})	0.36	0.45	0.39	0.37	0.42	0.49
	Area (%)	7.7 [a]	13.4 [a]	17.1 [a]	26.8 [a]	39.7 [a]	44.8 [a]
Doublet (2) Octahedral $[^{IV}Fe^{3+}\ 3Si^{4+}]$-$(3^{VI}Fe^{3+})$	δ (mm s^{-1})	0.47	0.47	0.47	0.46	0.45	0.45
	Δ (mm s^{-1})	0.63	0.69	0.66	0.70	0.76	0.84
	Width (mm s^{-1})	0.35	0.40	0.40	0.38	0.39	0.46
	Area (%)	27.6 [a]	32.0 [a]	33.2 [a]	34.0 [a]	31.4 [a]	30.1 [a]
Doublet (3) Octahedral $[2^{IV}Fe^{3+}\ 2Si^{4+}]$-$(3^{VI}Fe^{3+})$	δ (mm s^{-1})	0.44	0.44	0.45	0.45	0.45	0.45
	Δ (mm s^{-1})	1.15	1.16	1.09	1.18	1.23	1.27
	Width (mm s^{-1})	0.40	0.42	0.47	0.40	0.35	0.39
	Area (%)	25.2 [a]	19.3 [a]	16.6 [a]	11.0 [a]	6.4 [a]	5.0 [a]
Doublet (4) Tetrahedral $[3Si^{4+}]$-$(2^{VI}Fe^{3+})$	δ (mm s^{-1})	0.30	0.28	0.26	0.26	0.26	0.26
	Δ (mm s^{-1})	0.62	0.64	0.61	0.60	0.62	0.64
	Width (mm s^{-1})	0.41	0.43	0.45	0.42	0.42	0.45
	Area (%)	39.5 [a]	35.2 [a]	33.1 [a]	28.3 [a]	22.5 [a]	20.2 [a]
χ^2		3.50	2.23	1.24	1.22	1.47	1.59

[a]: *constrained parameter (± 5% of the theoretical area value of doublets determined from the structural model).*

This is a preprint, the final version is subject to change, of the American Mineralogist (MSA)
Cite as Authors (Year) Title. American Mineralogist, in press.
(DOI will not work until issue is live.) DOI: http://dx.doi.org/10.2138/am-2017-6039

Table 6: Sources and compositions of the reference natural nontronites.

Source		Composition per $O_{10}(OH)_2$	Reference
Koegas, Cape Province, South Africa	KOE	$Si_{3.3}\,Al_{0.04}\,Fe(III)_{2.69}\,Mg_{0.03}$	Goodman et al. (1976)
Garfield, Washington, U.S.A.	GAR	$Si_{3.42}\,Al_{0.53}\,Fe(III)_{2.03}\,Mg_{0.02}$	Goodman et al. (1976)
Manito, Washington, U.S.A.	MAN	$Si_{3.5}\,Al_{0.64}\,Fe(III)_{1.82}\,Mg_{0.05}$	Cardile and Johnston (1985)
Bingham Canyon, Utah, U.S.A	BIN	$Si_{3.49}\,Al_{0.94}\,Fe(III)_{1.46}\,Mg_{0.14}$	Cardile and Johnston (1985)
Spokane County, Washington, U.S.A.	SPO	$Si_{3.7}\,Al_{0.03}\,Fe(III)_{2.19}\,Mg_{0.03}$	Cardile and Johnston (1985)
Hohen Hagen, Germany	NG-1	$Si_{3.65}\,Al_{0.48}\,Fe(III)_{1.86}\,Mg_{0.03}$	Manceau (2000)
Uley Mine, South Australia, Australia	NAu-1	$Si_{3.49}\,Al_{0.66}\,Fe(III)_{1.84}\,Mg_{0.02}$	Keeling et al. (2000)
Uley Mine, South Australia, Australia	NAu-2	$Si_{3.78}\,Al_{0.25}\,Fe(III)_{1.92}\,Mg_{0.03}$	Gates et al. (2002)
Clausthal-Zellerfeld, Germany	CLA	$Si_{3.4}\,Al_{0.07}\,Fe(III)_{2.53}\,Mg_{0.03}$	Goodman et al. (1976)
Penge, Cape Province, South Africa	AMO	$Si_{3.42}\,Al_{0.02}\,Fe(III)_{2.58}\,Mg_{0.05}$	Goodman et al. (1976)
Koegas, Cape Province, South Africa	CRO	$Si_{3.38}\,Al_{0.03}\,Fe(III)_{2.39}\,Mg_{0.12}$	Goodman et al. (1976)

Table 7: Mössbauer parameters of the 298 K Mössbauer spectra of reference natural nontronite samples using the distribution model for tetrahedral substitutions (See text).

		GAR	**KOE**	**MAN**	**SPO**	**NG-1**	**NAu-1**	**BIN**	**NAu-2**
Doublet (1) Octahedral $[4Si^{4+}]$-$(3^{VI}Fe^{3+})$	δ (mm s^{-1})	0.37	0.39	0.36	0.38	0.38	0.37	0.36	0.37
	Δ (mm s^{-1})	0.22	0.25	0.22	0.32	0.33	0.25	0.22	0.22
	Width (mm s^{-1})	0.33	0.26	0.34	0.40	0.40	0.39	0.35	0.35
	Area (%)	49.5 [a]	32.7 [a]	56.4 [a]	62.9 [a]	62.1 [a]	56.7 [a]	55.2 [a]	70.4 [a]
Doublet (2) Octahedral $[^{IV}Fe^{3+}\ 3Si^{4+}]$-$(3^{VI}Fe^{3+})$	δ (mm s^{-1})	0.37	0.39	0.36	0.38	0.38	0.37	0.36	0.36
	Δ (mm s^{-1})	0.58	0.54	0.58	0.61	0.63	0.58	0.58	0.60
	Width (mm s^{-1})	0.31	0.26	0.29	0.30	0.30	0.33	0.29	0.34
	Area (%)	39.6 [a]	34.0 [a]	37.5 [a]	23.0 [a]	22.1 [a]	37.2 [a]	38.3 [a]	17.9 [a]
Doublet (3) Octahedral $[2^{IV}Fe^{3+}\ 2Si^{4+}]$-$(3^{VI}Fe^{3+})$	δ (mm s^{-1})	0.36	0.37	0.36	0.38	0.36	0.37	0.36	0.36
	Δ (mm s^{-1})	0.85	0.87	0.87	0.92	0.93	0.92	0.87	0.93
	Width (mm s^{-1})	0.27	0.35	0.27	0.30	0.33	0.40	0.27	0.27
	Area (%)	8.1 [a]	9.1 [a]	6.2 [a]	2.0 [a]	2.0 [a]	6.1 [a]	6.5 [a]	1.3 [a]
Doublet (4) Tetrahedral $[3Si^{4+}]$-$(2^{VI}Fe^{3+})$	δ (mm s^{-1})	0.18	0.21	-	0.19	0.17	-	-	0.17
	Δ (mm s^{-1})	0.47	0.49	-	0.54	0.55	-	-	0.53
	Width (mm s^{-1})	0.26	0.28	-	0.36	0.30	-	-	0.26
	Area (%)	2.7	24.3	0.0	12.1	13.8	0.0	0.0	2.4
χ^2		0.28	0.32	0.55	0.23	0.62	0.36	0.36	0.19

Note(s): For sample NAu-2, an extra doublet with the Mössbauer parameters given by Cashion et al. (2011), possibly due to non-structural iron, was used for the deconvolution (see text). [a]*: constrained parameter (± 5% of the theoretical area value of doublets determined from the structural model).*

This is a preprint, the final version is subject to change, of the American Mineralogist (MSA)
Cite as Authors (Year) Title. American Mineralogist, in press.
(DOI will not work until issue is live.) DOI: http://dx.doi.org/10.2138/am-2017-6039

Table 8: Mössbauer parameters of the 77 K Mössbauer spectra of reference natural nontronite samples using the distribution model for tetrahedral substitutions (See text).

		GAR	**KOE**	**CLA**	**CRO**	**AMO**
Doublet (1) Octahedral $[4Si^{4+}]$-$(3^{VI}Fe^{3+})$	δ (mm s^{-1})	0.49	0.50	0.51	0.50	0.48
	Δ (mm s^{-1})	0.23	0.24	0.26	0.27	0.29
	Width (mm s^{-1})	0.29	0.27	0.30	0.29	0.29
	Area (%)	49.5 [a]	32.7 [a]	39.1 [a]	35.7 [a]	39.9 [a]
Doublet (2) Octahedral $[^{IV}Fe^{3+}\ 3Si^{4+}]$-$(3^{VI}Fe^{3+})$	δ (mm s^{-1})	0.48	0.50	0.51	0.50	0.49
	Δ (mm s^{-1})	0.58	0.54	0.58	0.57	0.59
	Width (mm s^{-1})	0.28	0.27	0.29	0.29	0.28
	Area (%)	39.6 [a]	34.0 [a]	33.1 [a]	32.3 [a]	31.8 [a]
Doublet (3) Octahedral $[2^{IV}Fe^{3+}\ 2Si^{4+}]$-$(3^{VI}Fe^{3+})$	δ (mm s^{-1})	0.48	0.48	0.49	0.48	0.48
	Δ (mm s^{-1})	0.85	0.87	0.87	0.87	0.87
	Width (mm s^{-1})	0.27	0.37	0.37	0.35	0.37
	Area (%)	8.1 [a]	9.1 [a]	7.0 [a]	7.3 [a]	6.5 [a]
Doublet (4) Tetrahedral $[3Si^{4+}]$-$(2^{VI}Fe^{3+})$	δ (mm s^{-1})	0.31	0.31	0.32	0.31	0.30
	Δ (mm s^{-1})	0.47	0.51	0.55	0.53	0.53
	Width (mm s^{-1})	0.25	0.28	0.34	0.35	0.33
	Area (%)	2.7	24.3	20.8	24.7	21.8
χ^2		0.22	0.29	0.27	0.21	0.17

[a]*: constrained parameter (± 5% of the theoretical area value of doublets determined from the structural model).*

This is a preprint, the final version is subject to change, of the American Mineralogist (MSA)
Cite as Authors (Year) Title. American Mineralogist, in press.
(DOI will not work until issue is live.) DOI: http://dx.doi.org/10.2138/am-2017-6039

Table 9: $^{[4]}$Fe(III) content (in at.% of total Fe(III)) of the reference natural nontronite samples.

	GAR	**KOE**	**MAN**	**SPO**	**NG-1**	**NAu-1**	**NAu-2**	**BIN**	**CLA**	**CRO**	**AMO**
This study	2.7	24.3	0.0	12.1	13.8	0.0	2.6	0.0	20.8	24.7	21.8
Goodman et al. (1976)	9.0	27.0	-	-	-	-	-	-	15.0	19.0	28.0
Johnston and Cardile (1985)	9.0	-	-	-	-	-	-	-	-	-	-
Cardile and Johnston (1985)	-	21.0	9.0	7.0	-	-	-	4.0	-	-	-
Luca (1991)	2.0	23.0	-	5.6	16.0	-	-	5.0	-	-	-
Friedlander et al. (2015)	-	-	-	-	-	0.0	-	-	-	-	-
Cashion et al. (2011)	-	-	-	-	-	-	5				
Gates et al. (2002)	2.7	-	3.3	15.3	16.1	1.9	7.6	6.5	-	-	-
Manceau et al. (2000)	0.0	-	-	17.0	-	-	-	-	-	-	-
From the Kd approach of Decarreau and Petit (2014)	5.0	27.0	2.0	10.0	1.0	2.0	1.4	1.0	22.0	21.0	25.0

Note(s): For the Kd approach, the Kd value was 0.006.

List of Figure captions :

Figure 1: Example of the modeling (NT3 sample x = 0.77) of the distribution of $^{[4]}$Fe(III) substitutions in the two tetrahedral sheets of the layer (a and c) and tetrahedral neighbors to the $^{[6]}$Fe(III) cations in a *trans* vacant octahedral sheet (b) for a one-layer simulation. For details, see text.

Figure 2: Schematic of the tetrahedral sheet for the building of the distribution of $^{[4]}$Fe(III) substitutions.

Figure 3: Mössbauer spectra at 298 K of the synthetic nontronite samples. The spectral deconvolutions were made using four doublets corresponding to one tetrahedral and three octahedral environments (see text for details).

Figure 4: Mössbauer spectra at 77 K of the synthetic nontronite samples. The spectral deconvolutions were made using four doublets corresponding to one tetrahedral and three octahedral environments (see text for details).

Figure 5: Mössbauer spectra at 4 K of the synthetic nontronite samples.

Figure 6: Deconvolution of the Mössbauer spectra of the NT3 and the NT6 nontronite samples using three doublets corresponding to one tetrahedral and two octahedral environments. The arrows note the misfit between the experimental data and the fitted line from the three doublets.

Figure 7: Local cationic environment of an octahedral cation in a nontronite structure (a), each octahedral cation (in dark grey) is linked to three neighboring octahedrons and four neighboring tetrahedrons (two being up and two being down). Local cationic environment of a tetrahedral cation in a nontronite structure (b), each tetrahedral cation (in dark grey) is linked to two neighboring octahedrons and three neighboring tetrahedrons.

Figure 8: Deconvolution of the reconstructed experimental Mössbauer spectra of the Koegas (KOE) and Garfield (GAR) natural nontronites using the approach developed from synthetic nontronite. The experimental 77 K Mössbauer spectra of the KOE and the GAR are from Goodman et al. (1976). The experimental 298 K Mössbauer spectra of the KOE and the GAR are from Cardile and Johnston (1985) and Johnston and Cardile (1985), respectively.

Figure 9: Deconvolution of the reconstructed experimental 298 K Mössbauer spectra of the reference natural nontronite samples from Cardile and Johnston (1985): Spokane (SPO), Bingham (BIN), Manito (MAN); from Luca (1991): Hohen Hagen (NG-1), from Friedlander et al. (2015): Uley (NAu-1); and from Cashion et al. (2011): Uley (NAu-2). The deconvolutions were made using the approach applied to the synthetic nontronite samples.

Figure 10: Deconvolution of the reconstructed experimental 77 K Mössbauer spectra of the nontronite samples from Goodman et al. (1976): Clausthal (CLA), the crocidolite deposit of Koegas (CRO), and the amosite deposit of Penge (AMO). The deconvolutions were made using the approach applied to the synthetic nontronite samples.

Figure 11: Quadrupole splitting and isomer shift for Fe(III) in synthetic nontronites (full symbols) and in reference natural nontronites (empty symbols). Black symbols: 298 K spectra; Grey symbols: 77 K spectra. Circles: [3Si]-(2$^{[6]}$Fe(III)) local cationic environment around a $^{[4]}$Fe(III); Squares, diamonds, and triangles: local cationic environments around a $^{[6]}$Fe(III); [4Si]-(3$^{[6]}$Fe(III), [$^{[4]}$Fe(III) 3Si^{4+}]-(3$^{[6]}$Fe(III)), and [2$^{[4]}$Fe(III) 2Si^{4+}]-(3$^{[6]}$Fe(III)), respectively. Dotted rectangles: ranges of quadrupole splitting and isomer shift for $^{[4]}$Fe(III) and $^{[6]}$Fe(III) in silicate minerals (Coey, 1984).

Figure 12: Quadrupole splitting at 298 and 77 K vs. the full width at half maximum (FWHM) of the XRD (*06-33*) reflection of synthetic nontronites. Circles: local cationic environment around a $^{[4]}$Fe(III); [3Si]-(2$^{[6]}$Fe(III)). Squares, diamonds, and triangles: local cationic environments around a $^{[6]}$Fe(III); [4Si]-(3$^{[6]}$Fe(III), [$^{[4]}$Fe(III) 3Si^{4+}]-(3$^{[6]}$Fe(III)), and [2$^{[4]}$Fe(III) 2Si^{4+}]-(3$^{[6]}$Fe(III)), respectively.

This is a preprint, the final version is subject to change, of the American Mineralogist (MSA)
Cite as Authors (Year) Title. American Mineralogist, in press.
(DOI will not work until issue is live.) DOI: http://dx.doi.org/10.2138/am-2017-6039

Figure 1

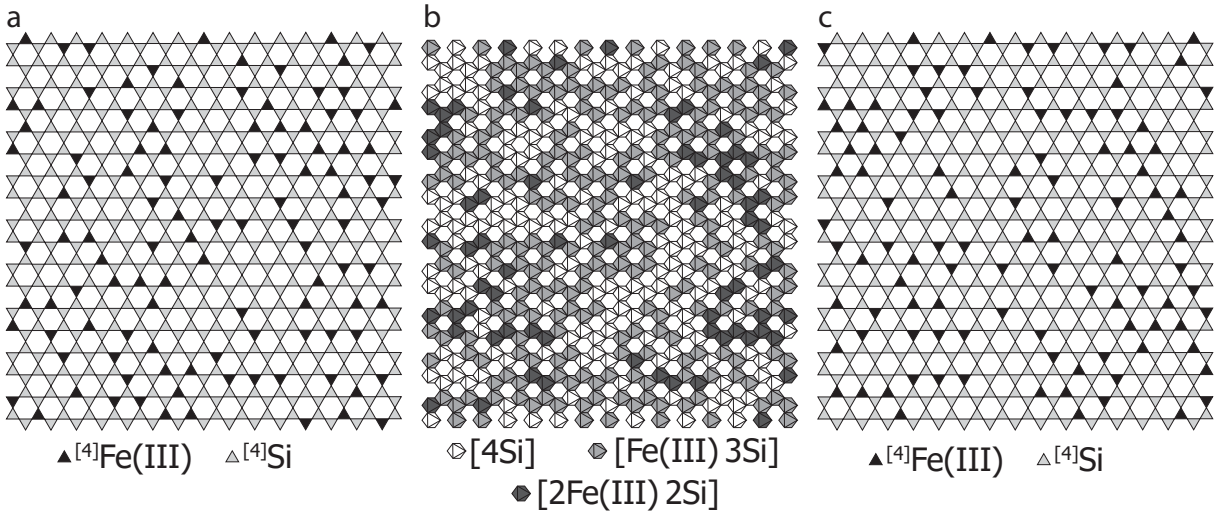

This is a preprint, the final version is subject to change, of the American Mineralogist (MSA)
Cite as Authors (Year) Title. American Mineralogist, in press.
(DOI will not work until issue is live.) DOI: http://dx.doi.org/10.2138/am-2017-6039

Figure 2

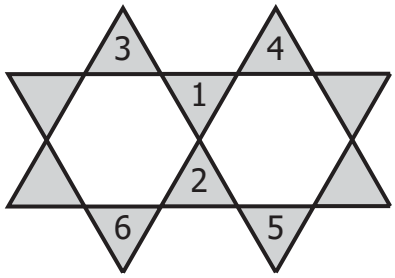

This is a preprint, the final version is subject to change, of the American Mineralogist (MSA)
Cite as Authors (Year) Title. American Mineralogist, in press.
(DOI will not work until issue is live.) DOI: http://dx.doi.org/10.2138/am-2017-6039

Figure 3

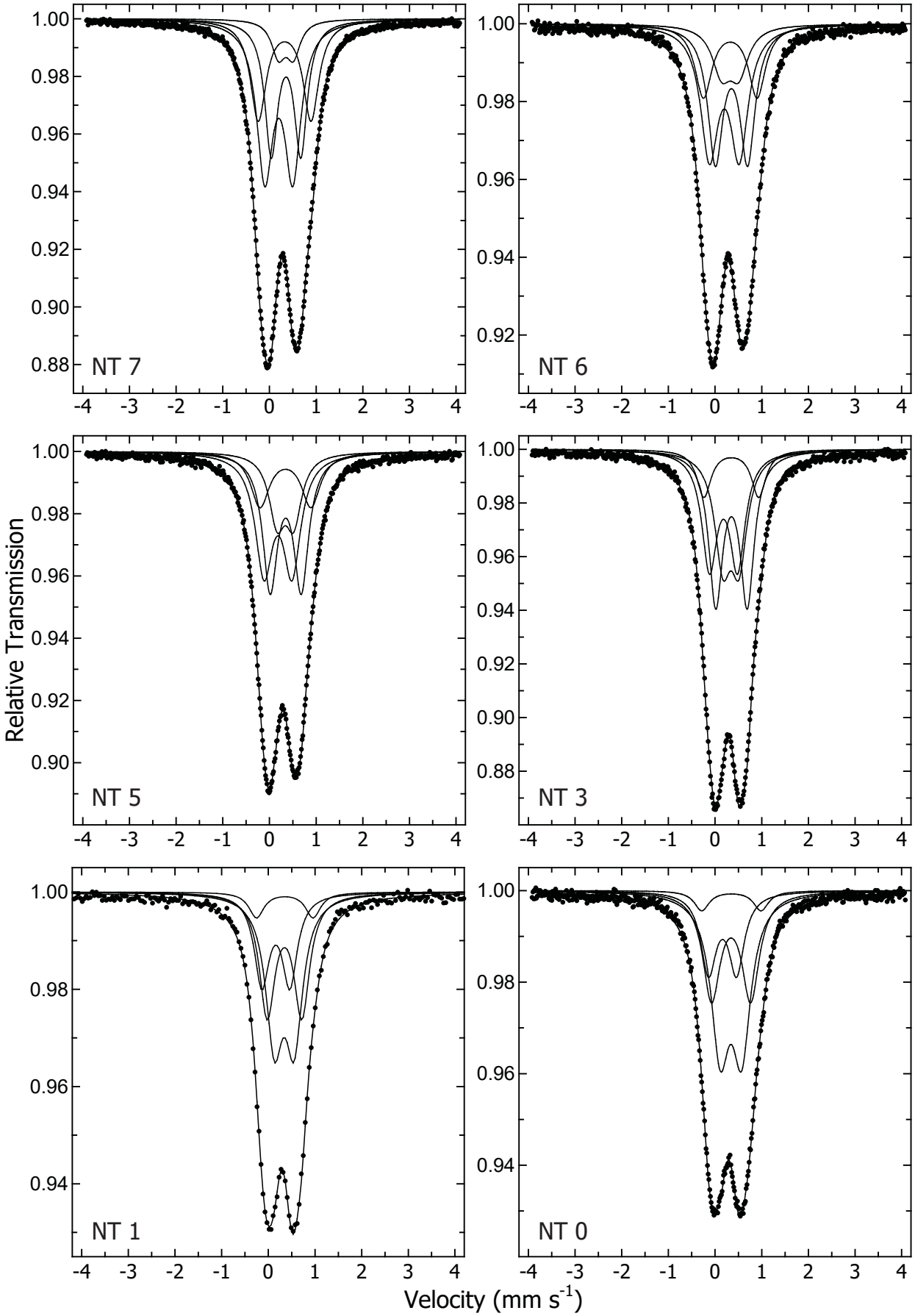

This is a preprint, the final version is subject to change, of the American Mineralogist (MSA)
Cite as Authors (Year) Title. American Mineralogist, in press.
(DOI will not work until issue is live.) DOI: http://dx.doi.org/10.2138/am-2017-6039

Figure 4

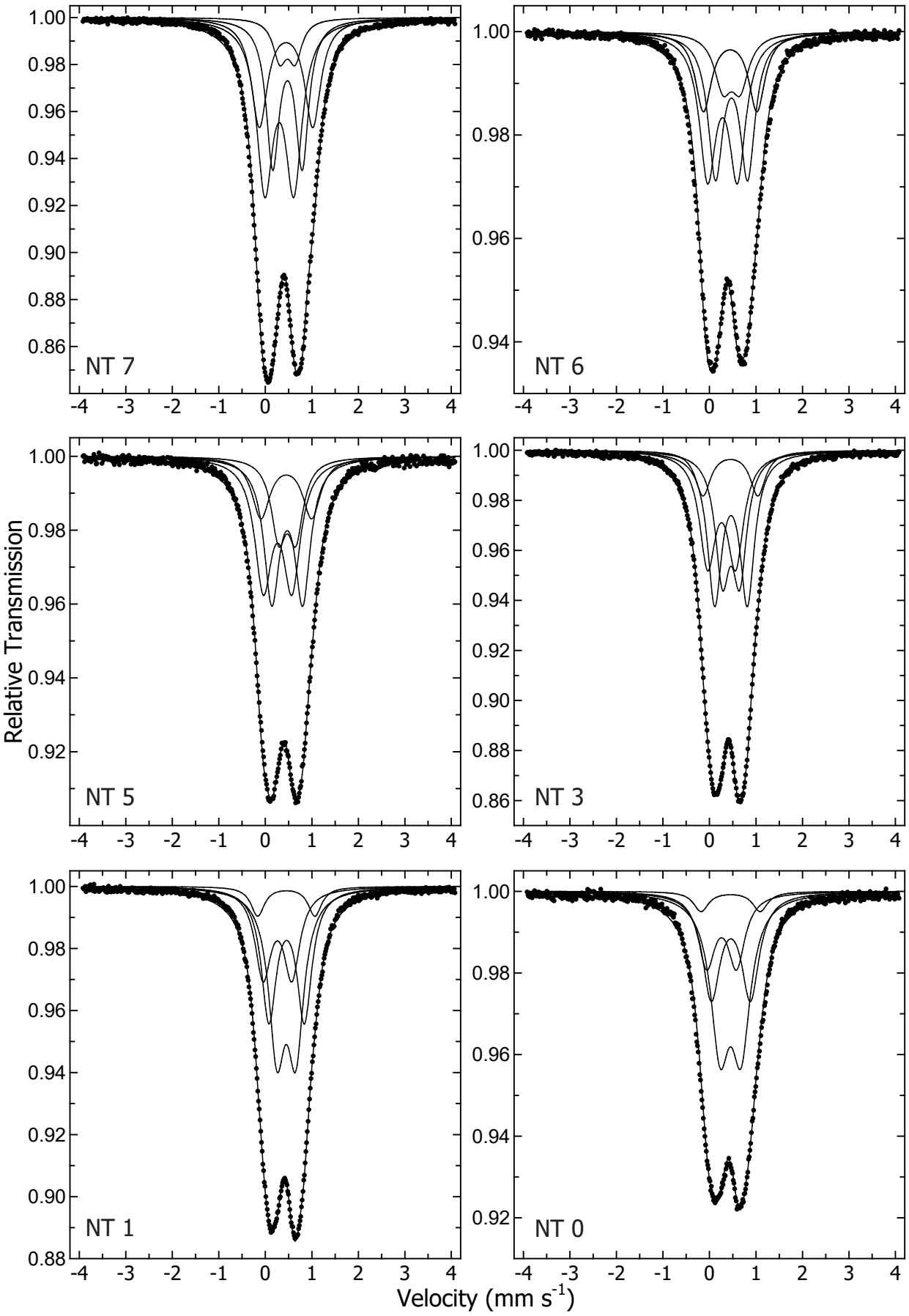

This is a preprint, the final version is subject to change, of the American Mineralogist (MSA)
Cite as Authors (Year) Title. American Mineralogist, in press.
(DOI will not work until issue is live.) DOI: http://dx.doi.org/10.2138/am-2017-6039

Figure 5

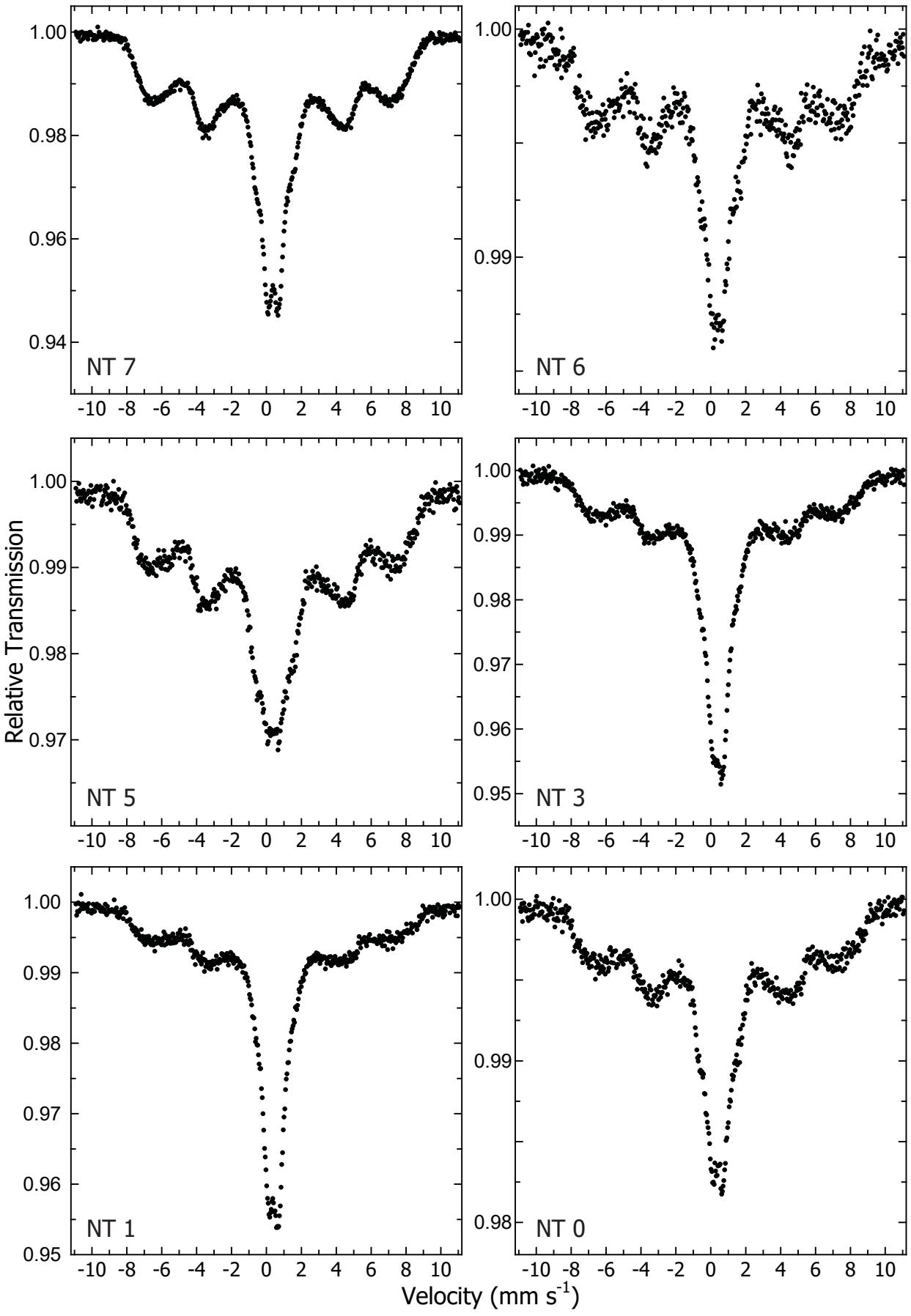

This is a preprint, the final version is subject to change, of the American Mineralogist (MSA)
Cite as Authors (Year) Title. American Mineralogist, in press.
(DOI will not work until issue is live.) DOI: http://dx.doi.org/10.2138/am-2017-6039

Figure 6

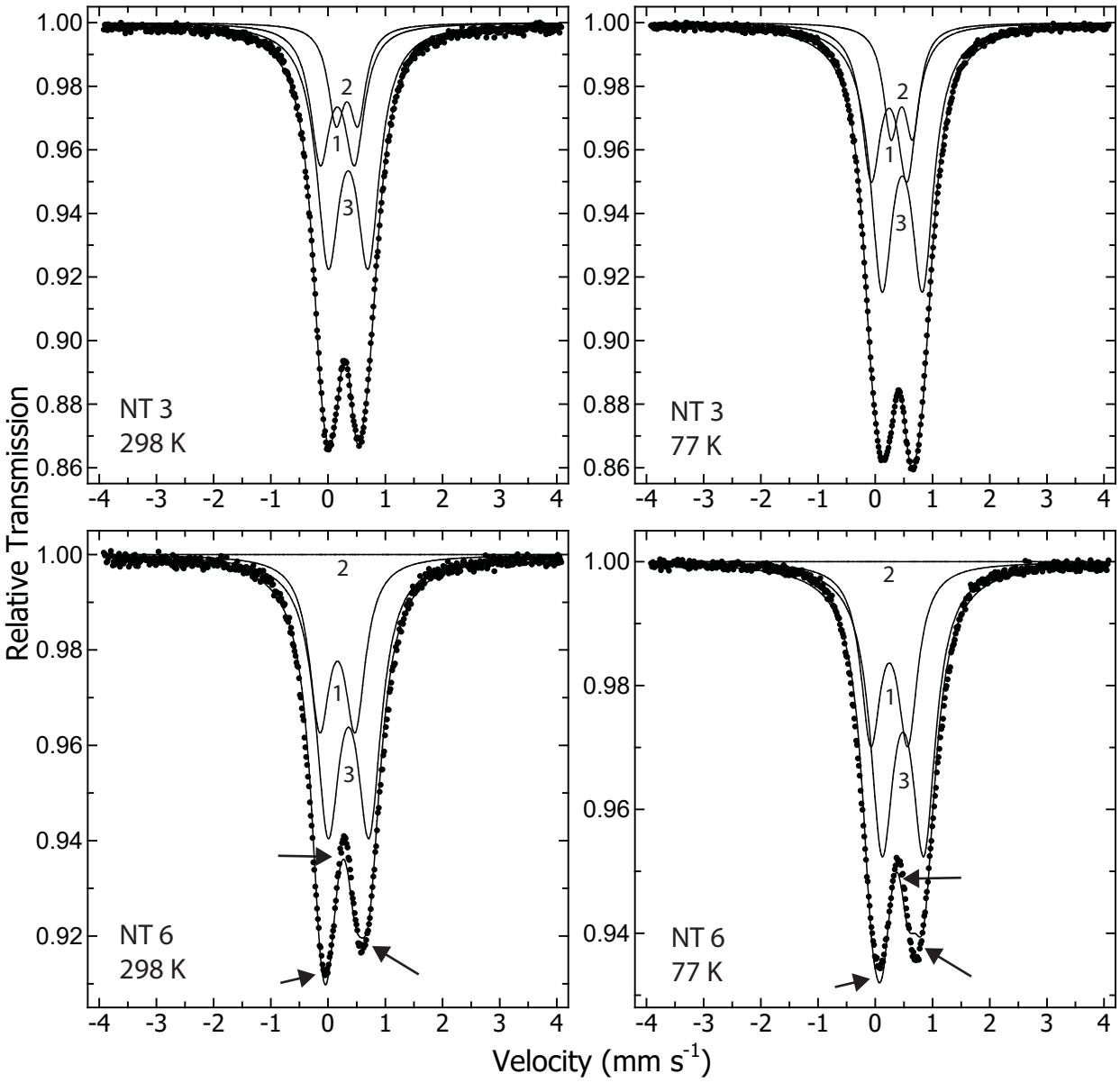

This is a preprint, the final version is subject to change, of the American Mineralogist (MSA)
Cite as Authors (Year) Title. American Mineralogist, in press.
(DOI will not work until issue is live.) DOI: http://dx.doi.org/10.2138/am-2017-6039

Figure 7

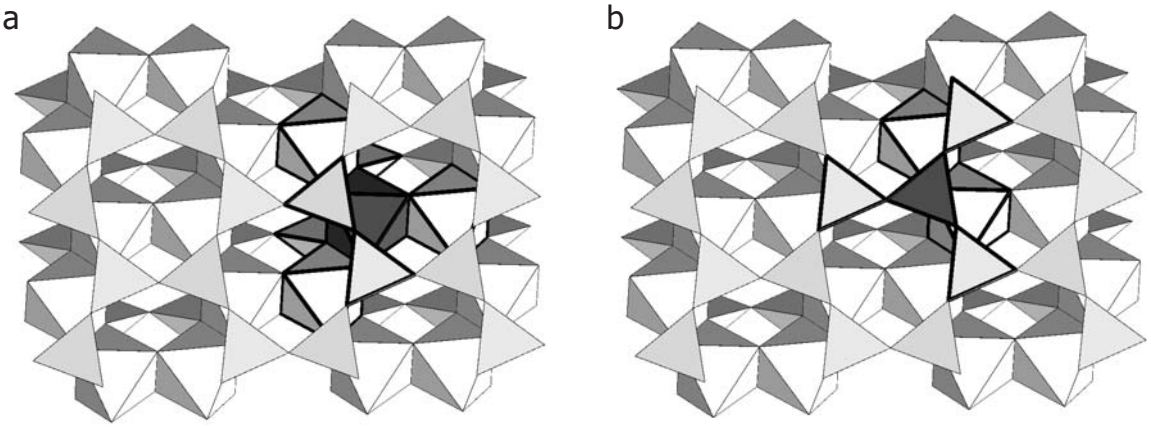

This is a preprint, the final version is subject to change, of the American Mineralogist (MSA)
Cite as Authors (Year) Title. American Mineralogist, in press.
(DOI will not work until issue is live.) DOI: http://dx.doi.org/10.2138/am-2017-6039

Figure 8

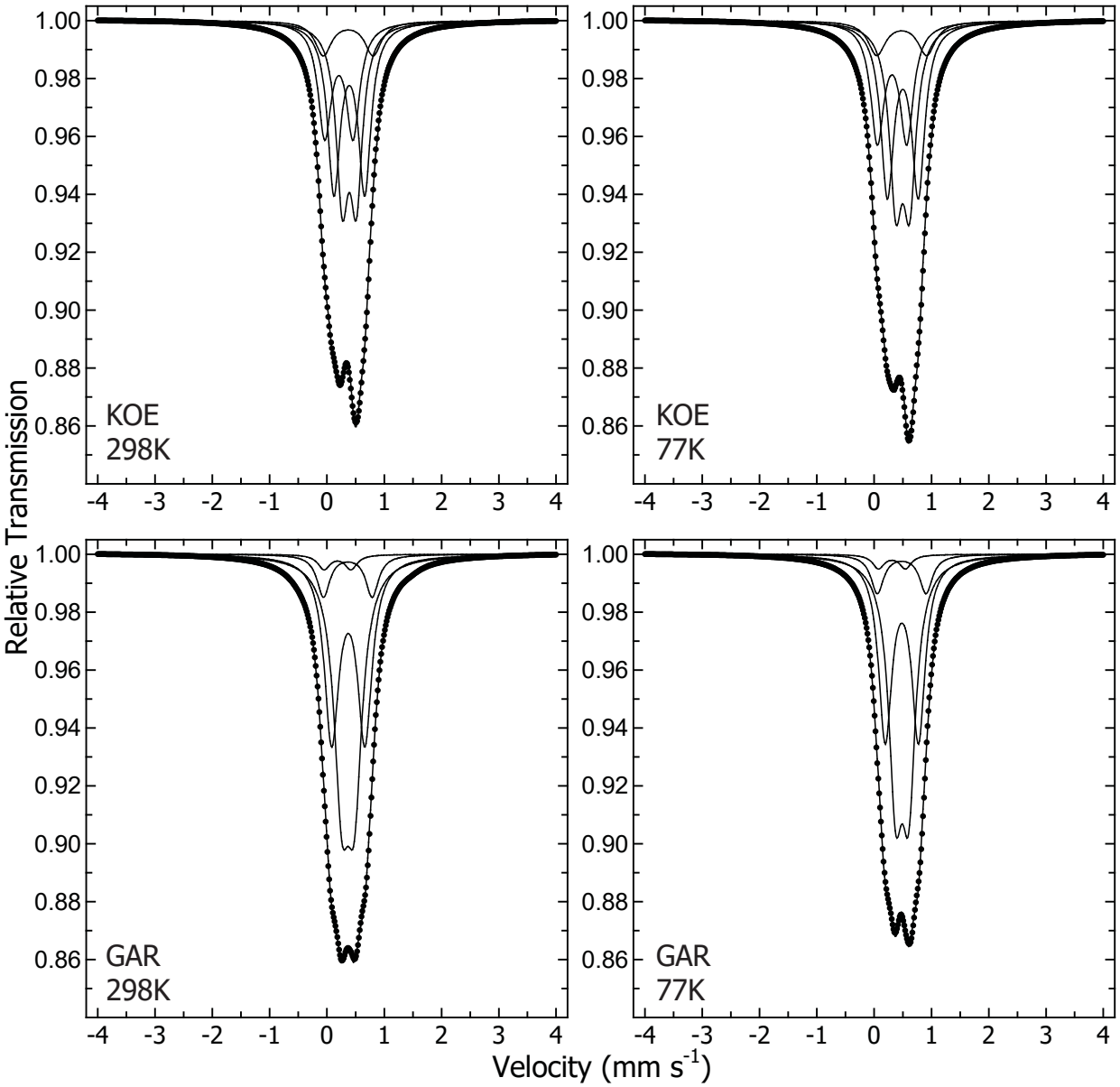

This is a preprint, the final version is subject to change, of the American Mineralogist (MSA)
Cite as Authors (Year) Title. American Mineralogist, in press.
(DOI will not work until issue is live.) DOI: http://dx.doi.org/10.2138/am-2017-6039

Figure 9

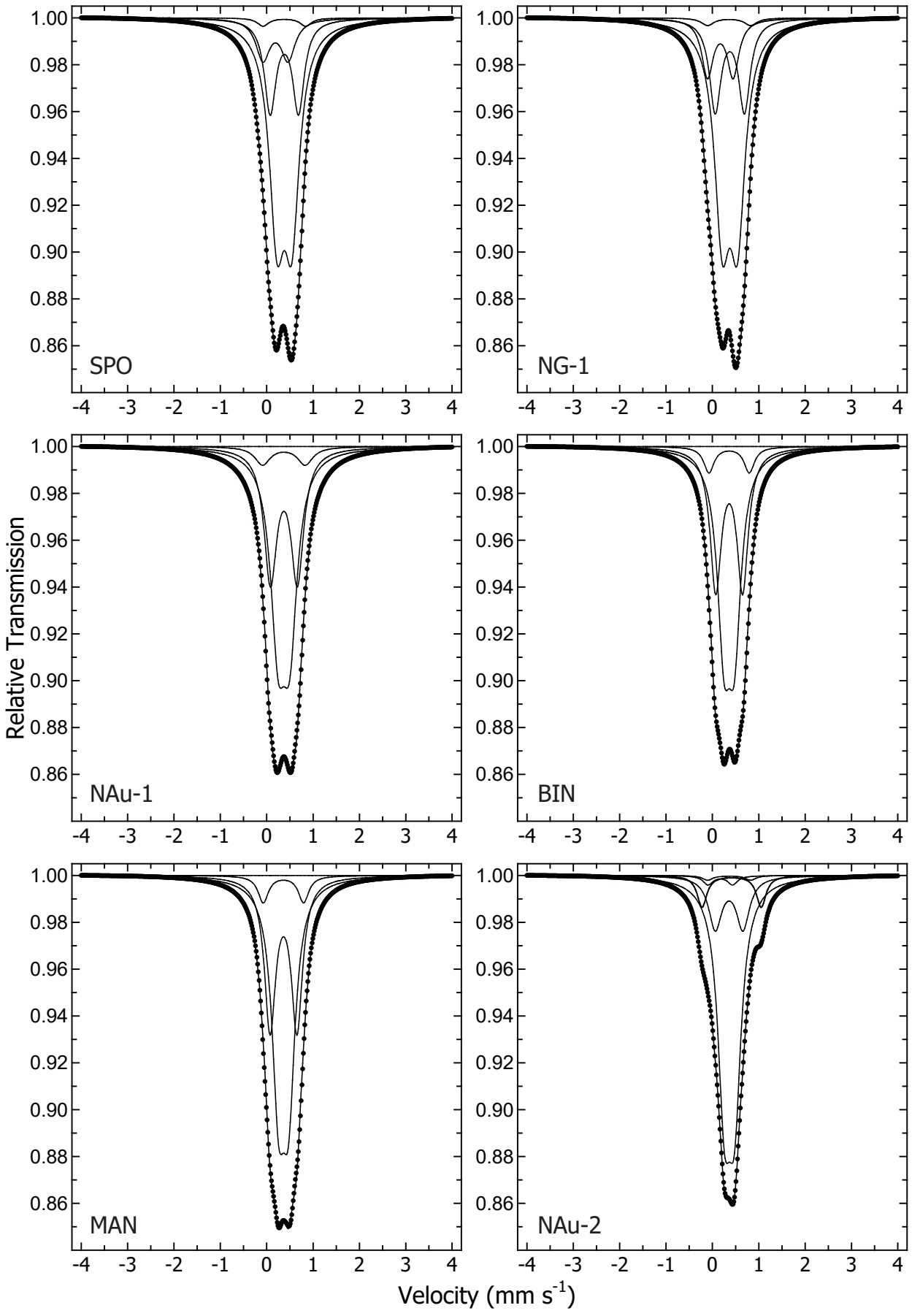

This is a preprint, the final version is subject to change, of the American Mineralogist (MSA)
Cite as Authors (Year) Title. American Mineralogist, in press.
(DOI will not work until issue is live.) DOI: http://dx.doi.org/10.2138/am-2017-6039

Figure 10

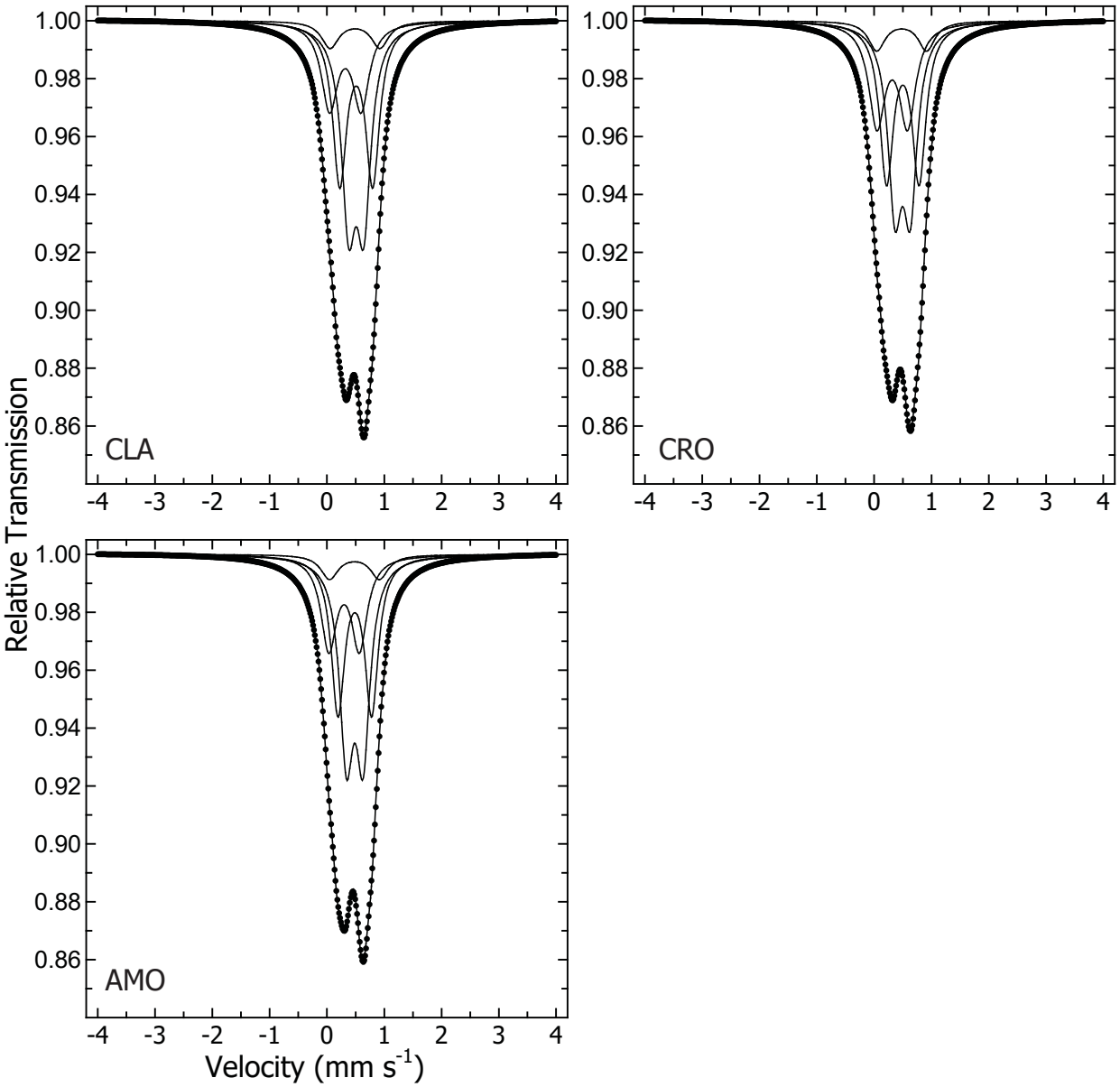

This is a preprint, the final version is subject to change, of the American Mineralogist (MSA)
Cite as Authors (Year) Title. American Mineralogist, in press.
(DOI will not work until issue is live.) DOI: http://dx.doi.org/10.2138/am-2017-6039

Figure 11

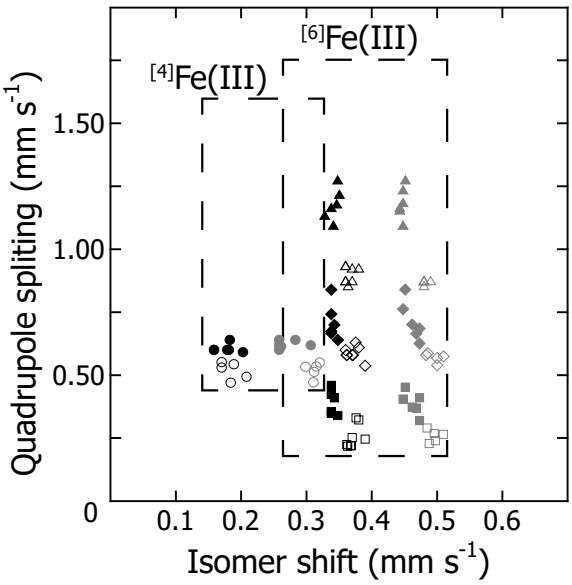

This is a preprint, the final version is subject to change, of the American Mineralogist (MSA)
Cite as Authors (Year) Title. American Mineralogist, in press.
(DOI will not work until issue is live.) DOI: http://dx.doi.org/10.2138/am-2017-6039

Figure 12